Journal of Geosciences, 61 (2016), 145–170 DOI: 10.3190/jgeosci.213

Original paper

Geochemical variability of granite dykes and small intrusions at the margin of the Granulite Complex in southern Bohemia

Radmila NAHODILOVÁ[1*], Stanislav VRÁNA[1], Jaroslava PERTOLDOVÁ[1], Petr GADAS[2]

[1] *Czech Geological Survey, Klárov 3, 118 21 Prague 1, Czech Republic; radmila.nahodilova@geology.cz*
[2] *Department of Geological Sciences, Masaryk University, Kotlářská 2, 611 37 Brno, Czech Republic*
**Corresponding author*

The study is focused on the composition of various types of Moldanubian dyke granites in the Bohemian Forest (Czech Republic). The studied area of about 200 km^2 is mainly in the northern environs of the Lipno dam lake on the Vltava River. This territory consists of metamorphic units such as Blanský les and Křišťanov granulite massifs associated with metasedimentary migmatite complexes of Monotonous and Varied units, intruded by Knížecí Stolec durbachite pluton and post-tectonic Variscan granitoids. The range of granite samples includes leucocratic rocks with muscovite, or with muscovite and biotite, and types with biotite as the single mica. Tourmaline- and garnet-bearing granites are less common. The set of 25 samples characterizes the composition of 20 dykes and small intrusions.

A simple provisional division of granite samples into low-Ca (0.35–0.65 wt. % CaO) and medium-Ca (0.67–1.16 wt. % CaO) groups is used. Tourmaline granites (± Ms, Grt) contain schorl with 20–40 mol. % dravite. Garnets contain almandine and spessartine as the major components (*c.* 30 mol. % Sps) but the sample from the Hrad hill exhibits an outer zone with up to 32 mol. % Grs. Apatite occurs in several generations, especially in low-Ca granites, which have a significant phosphorus substitution in feldspars: 1) primary fluorapatite, 2) minute anhedral apatite (containing P unmixed from albite) characterized by up to *c.* 10 mol. % of chlorapatite component in predominating fluorapatite, 3) very rare (hydrothermal) hydroxylapatite filling brittle fractures in tourmaline. Accessory cordierite, originally present in some leucogranites, is altered to pinite (muscovite + chlorite ± biotite aggregate). Several samples from the Smrčina area contained cordierite with low Be, which has been unmixed as a newly formed tiny beryl in pinite.

The dataset exhibits geochemical heterogeneity. Low-Ca and medium-Ca granites are distinct in the Ba–Rb–Sr ternary, as well as in the of Zr/Hf vs. Y/Ho and SiO_2 vs. A/CNK plots. The low-Ca dyke granites show numerous chemical differences from the granites of the plutonic bodies (such as the Eisgarn or Deštná types of the Moldanubian Batholith). The medium-Ca granite dykes split into the Smrčina type and remaining types of muscovite–biotite granites. Several types of chondrite-normalized REE patterns can be distinguished in terms of the total REE contents, the degree of LREE over HREE enrichment and magnitude of the Eu anomaly; most of the patterns show clearly a tetrad effect.

Keywords: granite, dykes and minor intrusions, geochemistry, petrology, Bohemian Massif, Moldanubian Zone
Received: 26 October, 2015; accepted: 30 April, 2016; handling editor: M. Štemprok
The online version of this article (doi: 10.3190/jgeosci.213) contains supplementary electronic material.

1. Introduction

The Moldanubian Batholith represents with its nearly 10 000 km^2 surface area the largest granitoid body in the Bohemian Massif. The Batholith consists of several major plutonic assemblages of Variscan age (Liew et al. 1989; Holub et al. 1995; Breiter 2010). Among these, the petrology, whole-rock geochemistry and genesis of anatectic (S-type) Eisgarn type granites has attracted a particular attention (e.g., Gerdes et al. 2000; René et al. 2008; Žák et al. 2011).

Numerous granite studies published during the last two decades on the Variscan plutons in southern Bohemia, Austria and Bavaria (see Klomínský et al. 2008; Žák et al. 2014 for review) cause an impression that the topics of granite petrology and geochemistry are well served. However, our reconnaissance study of dyke granites and small intrusions in course of geological mapping in northern environs of the Lipno dam lake in southern Bohemia has brought new interesting results (Pertoldová ed. 2006; Pertoldová and Nahodilová eds 2013). Their comparison with several groups of strongly fractionated late-stage stocks or small intrusions in a wider region shows that they represent yet another group of granitic rocks with poorly understood relations to plutonic geology, episodes of magma production and timing of emplacement. Data in this paper and their interpretation represent the first modern study of dyke granites in the Moldanubian Zone in southern Bohemia.

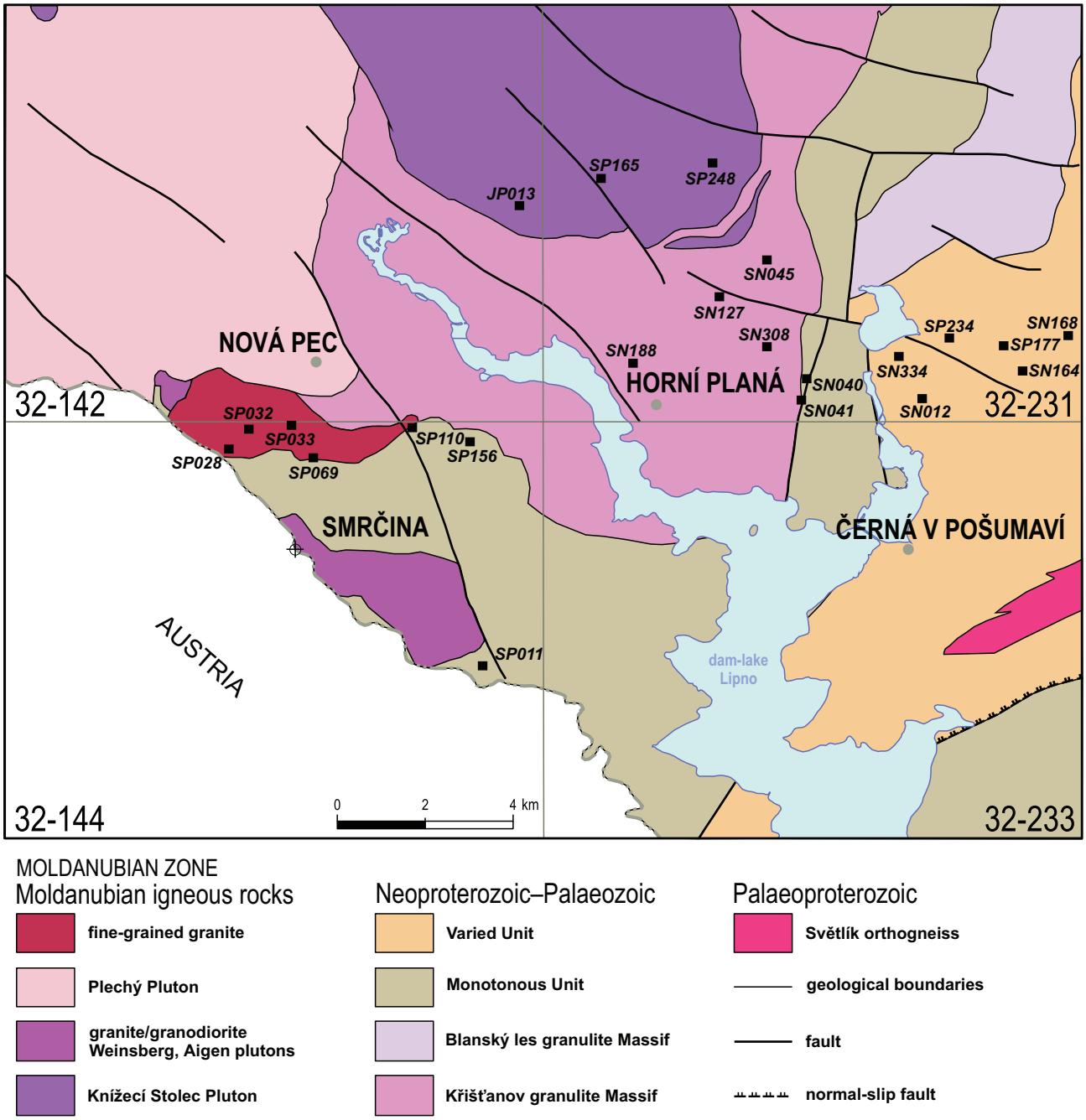

Fig. 1 Schematic geological map of the studied area, including parts of four Czech Geological Survey map sheets 1 : 25 000: 32-231 Horní Planá, 32-142 Nová Pec, 32-144 Smrčina and 32-233 Černá v Pošumaví.

2. Geological setting

Moldanubian Zone is formed by medium- to high-grade metamorphic rocks, interpreted as a tectonic melange of lower to middle continental crustal segments of the orogenic root (Schulmann et al. 2009) and intruded by numerous plutonic rocks from early Devonian calc-alkaline arc-type intrusions to late-tectonic Carboniferous granites (e.g. Finger et al. 1997; Holub 1997; Gerdes et al. 2000; Janoušek et al. 2000, 2004b and Žák et al. 2014).

The Moldanubian domain consists, from the top to the bottom, of the high-grade Gföhl Unit overlying the generally less metamorphosed Varied and Monotonous units (Fuchs 1976; Fuchs and Matura 1976; Thiele 1976, 1984). The Moldanubian Zone was affected by post-collision exhumation and intrusion of voluminous granitoids. The Moldanubian Batholith consists of the western and eastern branches of mostly allochthonous plutons (Klomínský et al. 2008). The study area is positioned where the two branches join.

Both the amphibolite-facies Monotonous and Varied units are dominated by sillimanite–biotite paragneisses, with minor orthogneiss and amphibolite bodies. As the name suggests, the Varied Unit is also characterized by the presence of marbles, quartzites, calc-silicate rocks, amphibolites and graphitic gneisses (Fiala et al. 1995). The Gföhl Unit comprises felsic and intermediate HP granulites accompanied by A-type eclogites, garnet pyroxenites and peridotites (Medaris et al. 1995), amphibolites accompanied by MORB eclogites (Štípská et al. 2014) and anatectic Gföhl orthogneisses (Hasalová et al. 2008).

2.1. Gneisses and migmatites of the Monotonous and Varied units

The rocks experienced tectonometamorphic evolution mainly under middle continental crust conditions. The metamorphism was followed by re-equilibration at high to moderate temperatures and low pressures, in particular around granite plutons. The main metamorphic events fall in the time-span of 341 to 325 Ma, which can be correlated with the Moravo-Moldanubian and Bavarian tectonometamorphic phases, respectively (Finger et al. 2007). Polyphase deformations were imprinted due to changes in the orientation and intensity of the regional stress field during uplift and regional shear deformations (e.g. Vrána 1979a; Vrána and Šrámek 1999; Finger et al. 2007). Dating of detrital zircons in paragneisses indicates a prevalence of ages in the range *c.* 580–520 Ma. Some samples from the Varied Unit contain also zircons of early Ordovician (Tremadocian) age (Košler et al. 2013).

2.2. Světlik orthogneiss

Amphibole–biotite orthogneiss of tonalite and quartz diorite composition, *c.* 8 by 3 km in an outcrop, is interpreted as an allochthonous segment of the Palaeoproterozoic crust onto which the Varied Group was originally deposited (Fiala et al. 1995). Zircon ages measured by several methods gave the protolith age of 2060–2100 Ma (Wendt et al. 1993; Fiala et al. 1995 and Trubač et al. 2012). High two-stage Nd model ages (T_{DM} = 3000 Ma; Liew and Hofmann 1988) support this interpretation. In course of the Variscan Orogeny, the rocks were deformed and metamorphosed jointly with the neighbouring gneisses and migmatites.

2.3. Granulites

Granulites carrying HP/HT record of metamorphism at the base of a thickened continental crust (P = 2.1–2.3 GPa, T = 950–1050 °C), were formed from felsic quartz–feldspathic rocks corresponding largely to granites (Fiala et al. 1987; Janoušek et al. 2004a; Vrána et al. 2013) at 341 to 339 Ma (Aftalion et al. 1989; Wendt et al 1994; Kröner et al. 2000; Svojtka et al. 2002; Sláma et al. 2007, 2008; O'Brien 2008). The granulite complex was rapidly uplifted to the level of the mid-continental crust, with resulting metamorphic re-equilibration. The Blanský les Granulite Massif is the largest unit in the granulite complex of southern Bohemia. It also contains granulite gneisses, bodies of mafic granulite, partly serpentinized garnet/spinel lherzolites dm to 2 km in outcrop size and boudins of eclogites. The Křišťanov Granulite Massif consists mostly of felsic granulites retrogressed to granulite gneisses.

2.4. Magmatic rocks of Variscan age

A concentric body of the Knížecí Stolec melanocratic amphibole–biotite syenogranite, accompanied by small satellite dykes, intruded the metamorphic rocks (Verner et al. 2008). It forms part of the durbachite suite that probably formed by mixing of magmas derived by partial melting of the enriched mantle with leucogranite melts (Holub 1997).

Granitoids of the Eisgarn and Weinsberg type (Plechý and Aigen plutons) also occur in the area (e.g. Gerdes et al. 2000; Pertoldová ed. 2006; Breiter et al. 2007). The Plechý Pluton at the western margin of the area of interest was studied recently by Pertoldová ed. (2006), Breiter et al. (2007), Siebel et al. (2006, 2008) and Verner et al. (2009). Syn- to post-tectonic emplacement and crystallization of the Plechý Pluton granitoids was dated to 327.1 ± 1.9 and 324.8 ± 3.4 Ma by Pb–Pb zircon evaporation method (Siebel et al. 2008).

Highly differentiated muscovite granite in the Homolka stock, SE of the study area, was dated at 319 ± 7 Ma by the whole-rock Rb–Sr method (Breiter and Scharbert 1995).Ten U–Pb dates of minerals of the columbite–tantalite group from rare-element pegmatites of western Moravia and southern Bohemia (Melleton at al. 2012) indicate two ages of emplacement: 1) an older episode at 333 ± 3 Ma for a majority of the Moravian localities; 2) a younger episode at 325 ± 4 Ma for Nová Ves in southern Bohemia and Ctidružice pegmatite in southern Moravia. With reference to Finger et al. (2007), the younger age is correlated with migmatization at the beginning of the Bavarian phase, whereas the older age closely follows the regionally widespread melting event that occurred at the end of the Moravo–Moldanubian phase.

3. Methods

3.1. Petrology and mineral chemistry

The study area is mainly on the northern environs of the Lipno dam lake on the Vltava River (Fig. 1). The samples

Tab. 1 Summary of studied granite samples

Sample ID	Locality	Outcrop type	Grain-size	Petrology	Modal composition, vol. %	wt. % CaO	Type of intrusives	Width, km	Length, km
SP110	U hájovny	b	fine-gr.	Ms–Bt granite	Bt 4, Ms 1	MCa; 1.00	intrusion	1.50	6.00
SP032	Studničná hora	b	fine-gr.	Bt–Ms granite	Ms 4, Bt 1, Tur 1	MCa; 0.91	intrusion	1.50	6.00
SP028	Studničná hora	b	small-gr.	Ms–Bt granite	Ms 3, Bt 3	MCa; 0.86	intrusion	0.20	0.50
SP069	Hraničník	b	fine-gr.	Ms granite with Bt	Ms 3, Bt 2	LCa; 0.48	intrusion	1.50	6.00
SP011C	Zadní Zvonková	o	fine-gr.	Bt granite	Bt 3	LCa; 0.41	dyke	0.02–0.03	0.40
SP033	Hraničník	b	fine-gr.	Ms–Bt granite	Bt 4, Ms 2	MCa; 0.93	intrusion	1.50	6.00
SP156	Šešovec	b	small-gr.	Tur granite with Ms and Grt	Ms 2, Tur, 3, Grt < 1	LCa; 0.35	dyke	0.05	0.80
SN045	Hodňov	o	fine-gr.	Ms–Bt granite	Bt. 4, Ms 2-3	LCa; 0.56	intrusion	0.20	0.50
SP177	Květušín	q	medium-gr.	Bt–Ms granite	Bt 3, Ms 4-5	MCa; 0.67	dyke	0.25	2.50
SP234	Květušín	q	medium-gr.	Bt–Ms granite	Bt 3, Ms 4-5	LCa; 0.59	dyke	0.12	2.20
SN168	Liščí díra	q	medium-gr.	Bt–Ms granite	Bt < 3, Ms 7	MCa; 0.68	dyke	0.10	1.00
SN012	Suchý vrch	o	medium-gr.	Ms granite with Bt	Bt 1, Ms 2-3	MCa; 1.16	dyke	0.13	1.70
SN040	Myslivecké údolí	o	small-gr.	Metagranite with Bt and Ms	Bt 2, Ms 1	LCa; 0.65	dyke	0.05	0.50
SN041A	Myslivecké údolí	q	medium-gr.	Bt granite with Ms	Bt 7, Ms < 2	MCa; 1.15	dyke	0.05	0.80
SP248	Liščí kámen	o	small-gr.	Bt–Ms granite	Bt 2, Ms 9	LCa; 0.41	intrusion	0.25	0.75
SN127	U tlustého Bártla	b	small-gr.	Bt–Ms granite with Tur	Bt < 3, Ms 5	LCa; 0.60	dyke	0.11	0.75
SN164A	Nad Skalným	b	small-gr.	Tur–Ms granite with Grt	Ms 8, Tur 7	LCa; 0.47	dyke	0.06	1.00
SN164B	Nad Skalným	b	small-gr.	Ms granite with Tur	Ms 3, Tur 2	LCa; 0.52	dyke	0.06	1.00
SN188	Horní Planá	o	small-gr.	Ms granite with Tur and Grt	Ms 3, Tur 2, Bt < 1, Grt < 1	LCa; 0.43	dyke	0.03	0.35
SP165	Nad Hospodárnicí	b	medium-gr.	Tur granite with Ms	Tur 7, Ms 1	LCa; 0.43	dyke	0.03	0.50
SN308	Hodňov	o	medium-gr.	Bt–Ms granite	Bt 2, Ms 3	LCa; 0.61	dyke	0.04	0.60
SN334A	Suchý vrch	o	fine-gr.	Ms granite with And	And 1, Ms 4	LCa; 0.48	dyke	0.03	0.50
SN334B	Suchý vrch	o	medium-gr.	Ms granite	Ms 3	LCa; 0.59	dyke	0.03	0.50
JP013A	Hrad	o	small-gr.	Granite with Bt and Grt	Bt < 2	MCa; 0.68	dyke	0.002	0.02
JP013B	Hrad	o	fine-gr.	Granite with Bt, Grt and Tur	Bt < 2	MCa; 0.71	dyke	0.005	0.04–0.05

Outcrop type: q = quarry, o = outcrop, b = blocks
MCa = medium-Ca granite, LCa = low-Ca granite

represent dykes and small intrusions in various geological units in the Šumava area, such as granulites, the Monotonous and Varied units and the amphibole–biotite syenitoid to melagranitoid pluton (durbachite). Geochemical and petrological data on 25 granite samples have been obtained in the course of geological mapping in the Moldanubian Zone of southern Bohemia (Pertoldová ed. 2006; Pertoldová and Nahodilová eds 2013). Samples were collected in quarries, outcrops and from large blocks (Tab. 1). The documentation of the sampling points is kept in the lithogeochemical database of the Czech Geological Survey.

After polished thin sections were studied using optical microscopy, full-size images of thin sections were scanned to expedite microprobe work. Chemical analyses of minerals were carried out with CAMECA SX 100 WDS electron microprobe in the Joint Laboratory of Electron Microscopy and Microanalysis, Department of Geological Sciences, Masaryk University and the Czech Geological Survey, Brno. The analytical conditions varied according to the mineral analyzed, usually involving 15 kV accelerating voltage, probe current of 10–20 nA and acquisition time of 10–30 s. The standards used were spessartine (Si, Mn), almandine (Fe), andradite (Ca), $MgAl_2O_4$ (Mg), hornblende (Ti), sanidine (Al, K), albite (Na), fluorapatite (P), chromite (Cr), other minerals containing REE and some minor elements. The raw data were reduced using PAP matrix corrections (Pouchou and Pichoir 1985).

3.2. Whole-rock geochemistry

For analyses were sampled completely fresh rocks free of weathering effects; samples (*c.* 10 kg)

were crushed in the laboratories of the Czech Geological Survey Prague–Barrandov (CGS) to grain fraction 2–4 cm by steel jaw crusher, homogenized and split to 500–1500 g. Finally, aliquots of *c.* 300 g were grinded in an agate mill. Selected major-element analyses were carried out by wet chemistry at CGS (Dempírová 2010). The relative 2σ uncertainties were better than 1 % (SiO_2), 2 % (FeOt), 5 % (Al_2O_3, K_2O, and Na_2O), 7 % (TiO_2, MnO, CaO), 6 % (MgO) and 10 % (Fe_2O_3, P_2O_5). The REE and other trace elements were analyzed at the Acme Analytical Laboratories (Vancouver) Ltd. and at the Activation Laboratories (Ancaster, Ontario) Ltd., both in Canada by ICP-MS following a lithium metaborate or tetraborate fusion and nitric acid digestion of a 0.2 g sample (method 4B). For further analytical details, see *http://acmelab.com*.

Recalculation and plotting of the whole-rock geochemical data were performed using the R language *GCDkit* package (Janoušek et al. 2006), version 3. Mineral formulae recalculation used largely worksheets presented on the web by A. Tindle. Mineral abbreviations in this paper follow Whitney and Evans (2010).

4. Results

4.1. Petrography

The studied granite samples (Fig. 1) exhibit geochemical and mineralogical heterogeneity. In Tab. 1 various types of granite dykes and small intrusions are classified in the following categories: a) minor dykes, less than 10 m wide, b) dykes 10–200 m wide, and c) small intrusions (characterized by their dimensions). The samples are muscovite granites, biotite–muscovite or muscovite–biotite granites or tourmaline–muscovite ± garnet granites (Tab. 1). Normative calculated composition (granite mesonorm) was tested, but owing to significant phosphorus partitioning not only into apatite, but also plagioclase and K-feldspar it gives misleading results. This results in erroneous Ca distribution between plagioclase and apatite.

In order to avoid these problems, a simple division of granite samples into low-Ca (0.35–0.65 wt. % CaO) and medium-Ca (0.67–1.16 wt. %) groups is used (Fig. 2a). Separation of the two granite types is documented also by the Ba–Rb–Sr diagram (Fig. 2b), and will be further addressed in the whole-rock geochemical section below.

Deformed, cataclastic rock types grading up to mortar structure and foliated fabric (samples SN012 Suchý vrch, SN040 Myslivecké údolí) are rare. Effects of local brittle deformation are common. Weakly porphyritic textures with small phenocrysts of K-feldspar up to 8 mm (SN041, SN012) are rare. Most common accessories are tourmaline, garnet, zircon, monazite, ilmenite (in part secondary); less common are rutile, xenotime, monazite, pyrite and arsenopyrite. Cordierite, altered to pinite pseudomorphs, is present in about one third of the samples.

4.2. Mineral chemistry

The chemical composition of minerals was analyzed with an electron microprobe in a majority of the samples. The tables of mineral analyses (Tabs 2–7) present selected typical compositions but the full variation is shown mainly in the diagrams.

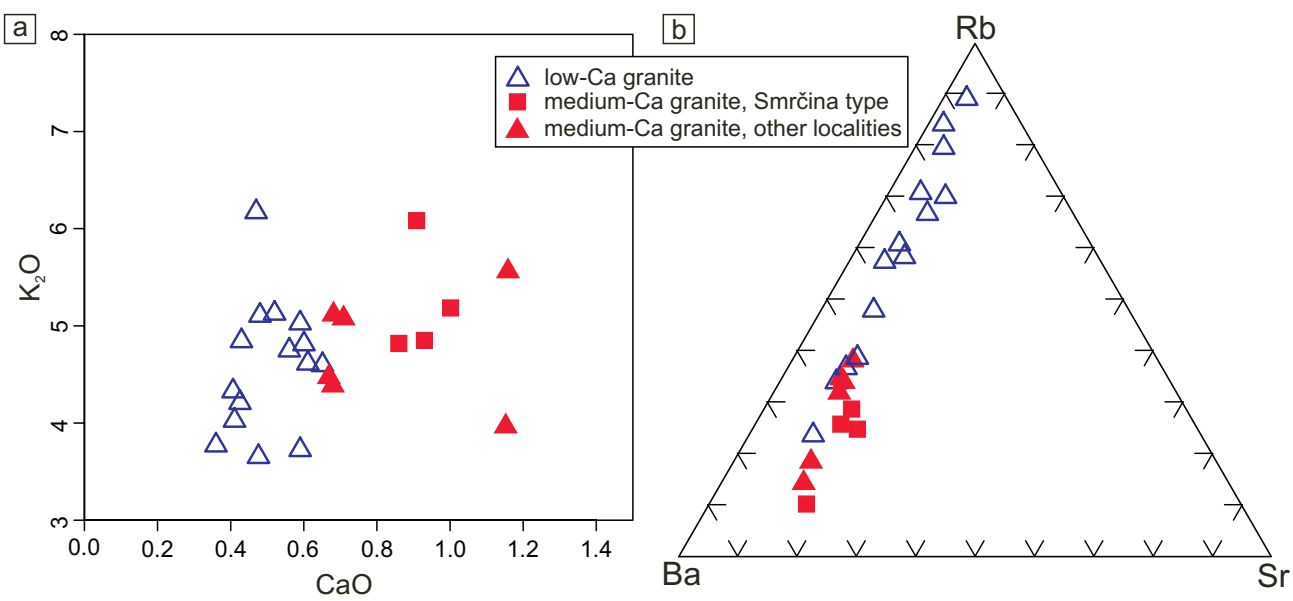

Fig. 2a – CaO vs. K_2O (wt. %) diagram for the studied granites; **b** – Ternary plot Ba–Rb–Sr (ppm).

Tab. 2 Electron-microprobe analyses of feldspars (wt. %)

mineral	Pl	Pl	Pl	Pl	Pl	Kfs	Kfs	Kfs	Kfs
sample	SN308	SN188	SN334A	SP234	SN012	SN188	JP013A	SP234	SN334B
analysis	15	29	41	70	101	1	1	2	1
SiO_2	64.81	67.94	65.47	65.95	62.68	64.25	64.83	64.20	63.91
Al_2O_3	21.54	19.77	21.65	21.5	22.95	18.51	18.64	18.65	18.48
Fe_2O_3	b.d.l.	0.22	b.d.l.	b.d.l.	b.d.l.	b.d.l.	b.d.l.	b.d.l.	b.d.l.
CaO	2.80	0.20	1.83	1.87	4.10	0.00	0.13	0.00	0.08
Na_2O	10.37	11.22	10.55	10.45	9.39	0.36	0.70	0.61	0.93
K_2O	0.23	0.07	0.34	0.21	0.13	16.65	16.02	16.23	15.75
BaO	0.00	0.00	0.00	0.00	0.02	0.00	0.22	0.00	0.27
P_2O_5	0.37	b.d.l.	0.57	0.19	0.17	0.36	0.11	0.38	0.15
Total	100.12	99.42	100.41	100.17	99.44	100.13	100.65	100.07	99.57
Number of atoms (per 8 O) (apfu)									
Si	2.866	2.984	2.865	2.89	2.789	2.972	2.981	2.967	2.973
Al	1.123	1.023	1.117	1.11	1.204	1.009	1.010	1.016	1.013
Fe^{3+}	–	0.007	–	–	–	–	–	–	–
Ca	0.099	0.009	0.086	0.088	0.191	0.000	0.006	0.000	0.004
Na	0.889	0.956	0.895	0.888	0.81	0.032	0.062	0.055	0.084
K	0.013	0.004	0.019	0.012	0.007	0.983	0.940	0.957	0.935
Ba	0.000	0.000	0.000	0.000	0.000	0.000	0.004	0.000	0.005
P	0.014	–	0.021	0.007	0.006	0.014	0.004	0.015	0.006
cat sum	5.003	4.984	5.002	4.994	5.008	5.010	5.008	5.009	5.020
End-members (mol. %)									
An	9.90	0.90	8.60	8.90	18.90	0.00	0.60	0.00	0.40
Ab	88.80	98.70	89.50	89.90	80.40	3.20	6.10	5.40	8.20
Or	1.30	0.40	1.90	1.20	0.70	96.80	92.90	94.60	91.00
Cls	0.00	0.00	0.00	0.00	0.00	0.00	0.40	0.00	0.50

b.d.l. = below detection limit

4.2.1. Plagioclase

Plagioclase compositions (Tab. 2) correspond to albite and oligoclase. The studied granites were provisionally classified to "low-Ca granites" and "medium-Ca granites" with the division at 0.65 wt % CaO; this CaO content corresponds approximately to albite $An_{9.7}$. Oligoclase with the maximum recorded Ca content, $An_{19.5}$, was analyzed in sample SN012. As is often the case with similar albite–oligoclase-rich peraluminous granites (Frýda and Breiter 1995), plagioclase contains significant quantity of phosphorus, ranging up to 0.021 apfu (0.57 wt. % P_2O_5) (Fig. 3). Several samples exhibit a phosphorus maximum with plagioclase composition in the range $An_{7.7–10.7}$. The potassium contents are variable both in albitic and oligoclase compositions and there is a poorly defined positive correlation between K_2O and CaO.

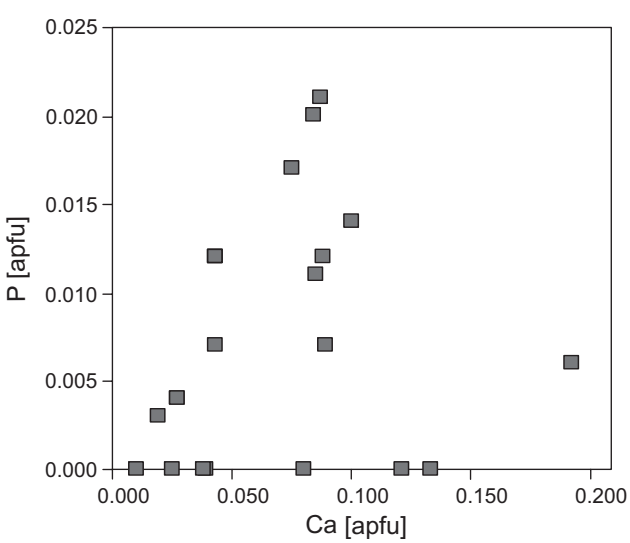

Fig. 3 Variation of Ca and P (apfu) in plagioclase.

The micro-porosity of albitic plagioclase on a micron-level, frequently observed in the course of microprobe work (see text on apatite), is a surprising phenomenon (Breiter et al. 2005). It is suggested somewhat tentatively that the porosity formation is in some way associated with phosphorus separation from plagioclase and the formation of tiny granules (< 1 micron) of a second-generation apatite in plagioclase.

4.2.2. K-feldspar

K-feldspars are usually anhedral to subhedral, weakly perthitic, in rare cases partly replaced by fine muscovite. Seven K-feldspar analyses contain 3–8 mol. % Ab, < 1 mol. % An and 0.004 to 0.015 apfu P (0.11 to 0.38

wt. % P_2O_5). Barium contents of 0–0.005 apfu correspond approximately to the whole-rock variation. Low barium contents are more typical of low-Ca granite samples.

4.2.3. Muscovite

Representative chemical compositions of muscovite are shown in Tab. 3. The Fe vs. Ti diagram supports the existence of a muscovite group that crystallized via replacement of biotite, as indicated by the correlation of elevated Fe and Ti contents, mainly in the range of 0.055–0.084 apfu Fe (Fig. 4). Other paragenetic types include a secondary muscovite in pinite pseudomorphs after cordierite, widely dispersed minute muscovite crystals in some plagioclase grains, and monomineral fine-grained muscovite aggregates (e.g. SN308 Hodňov). Possible primary muscovite is characterized by relatively coarse crystals and lack of structural indication of reaction relationship with the neighbouring minerals.

Tab. 3 Electron-microprobe analyses of muscovite and chlorite (wt. %)

mineral	Ms	Ms	Ms	Ms	Ms in pinite	Chl in pinite
sample	SP110A	SN188	SN308	SN334B	SN248	SN248
analysis	12	24	14	1	30	29
SiO_2	45.91	46.17	45.74	45.70	46.82	24.34
Al_2O_3	35.41	35.43	34.08	37.62	34.36	20.55
TiO_2	0.65	b.d.l.	b.d.l.	b.d.l.	b.d.l.	b.d.l.
FeOt	1.02	1.38	2.15	0.48	1.92	34.09
MnO	0.00	0.04	0.08	0.01	0.06	1.61
MgO	0.65	0.65	0.63	0.15	0.85	5.60
ZnO	0.00	0.00	0.04	0.00	0.00	b.d.l.
CaO	0.00	0.02	0.01	0.00	0.00	b.d.l.
Na_2O	0.51	0.61	0.17	0.33	0.27	b.d.l.
K_2O	10.68	10.69	11.19	11.08	10.79	0.24
BaO	b.d.l.	b.d.l.	b.d.l.	b.d.l.	b.d.l.	0.20
H_2O*	4.42	4.37	4.30	4.48	4.32	10.51
F	0.14	0.24	0.25	b.d.l.	0.33	b.d.l.
O=F	–0.06	–0.10	–0.11	–0.04	–0.14	0.00
Total	99.34	99.50	98.52	99.81	99.58	97.14
Number of ions on the basis of 12 (O, OH, F) and for chlorite of 14 (O, OH) (apfu)						
Si	3.069	3.087	3.110	3.030	3.132	2.778
Al	2.790	2.792	2.731	2.939	2.709	2.764
Ti	0.033	–	–	–	–	–
Fe^{2+}	0.057	0.077	0.122	0.027	0.107	3.254
Mn	0.000	0.002	0.005	0.000	0.003	0.156
Mg	0.065	0.065	0.064	0.015	0.085	0.861
Zn	0.000	0.000	0.002	0.000	0.000	–
Ca	0.000	0.001	0.001	0.000	0.000	–
Na	0.066	0.079	0.022	0.042	0.035	–
K	0.911	0.912	0.971	0.937	0.921	0.035
Ba	–	–	–	–	–	0.009
OH*	1.970	1.949	1.946	2.000	1.930	8.000
F	0.030	0.051	0.054	–	0.070	–
cat sum	6.991	7.016	7.027	6.990	6.992	9.857
Fe/(Fe+Mg)	0.467	0.542	0.656	0.643	0.557	0.790

Cr, Sr, Sn, Rb, Cs, Ga, Ni, Cu, V, P were also analyzed but the abundances are below detection limits
* calculated H_2O content
b.d.l. = below detection limit

4.2.4. Biotite

Representative chemical composition of biotite types in 14 analysed samples are shown in Tab. 4. The analyses are plotted in Al_{tot} vs. Fe/(Fe + Mg) binary plot (Fig. 5). The variation in Fe/(Fe + Mg) values indicates the existence of several compositional fields. For convenience of comparison with literature data (René et al. 2008) the Mg#, a complementary value to Fe/(Fe + Mg), is used in the following text.

The biotite group 1A with biotite Mg# 0.16–0.33 includes low-Ca granite samples. The group 1B with Mg# 0.32–0.40 corresponds to biotites from both, low-Ca and medium-Ca granites. Higher temperature biotites (René et al. 2008) of the group 2 include samples of medium-Ca granites with Mg# 0.53–0.58. One sample (group 3, SN012, Suchý vrch) with a surprisingly magnesian, high-T biotite (Mg# 0.69) stands aside as a specific rock type.

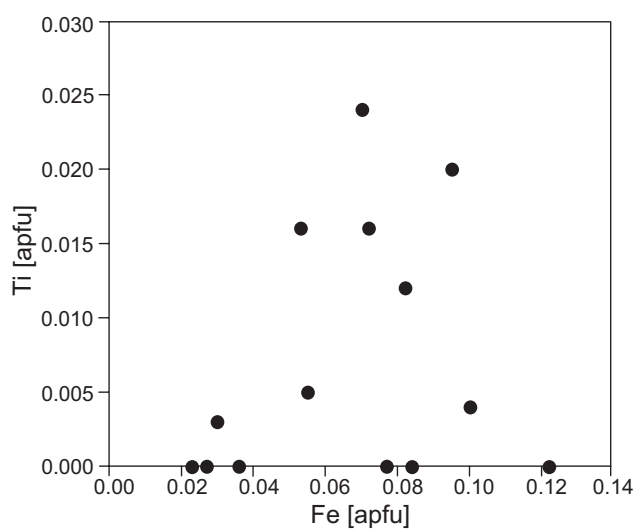

Fig. 4 Fe vs. Ti (apfu) in muscovite.

Tab. 4 Electron-microprobe analyses of biotite (wt. %)

sample	SN188	SN012	JP13B	SP177	SN110B	SP032
analysis	27	107	61	19	147	37
SiO_2	33.32	37.57	34.72	35.04	35.61	35.75
Al_2O_3	18.41	17.93	17.99	20.14	18.84	18.83
TiO_2	2.46	1.90	2.34	0.64	2.50	2.70
Cr_2O_3	0.00	0.04	0.02	0.01	0.08	0.01
FeOt	27.94	10.96	23.51	21.33	18.67	19.37
MnO	0.66	0.43	0.72	0.77	0.27	0.86
MgO	2.78	13.85	5.88	5.15	8.63	8.62
ZnO	0.02	0.07	0.09	0.10	0.05	0.06
CaO	0.01	0.02	0.01	0.01	0.01	0.01
Na_2O	0.08	0.07	0.05	0.03	0.08	0.03
K_2O	9.10	9.52	9.25	9.00	9.64	9.50
BaO	0.00	0.00	0.13	0.00	0.18	0.02
Rb_2O	0.10	0.01	0.10	0.00	0.00	0.00
Cs_2O	0.04	0.00	0.00	0.00	0.00	0.00
V_2O_3	0.05	0.08	0.01	0.01	0.11	0.04
Sc_2O_3	0.01	0.04	0.01	0.00	0.00	0.00
P_2O_5	0.00	0.00	0.00	0.01	0.00	0.00
H_2O*	3.59	3.47	3.53	3.43	3.73	3.78
F	0.29	1.07	0.59	0.75	0.37	0.35
Cl	0.02	0.01	0.01	0.00	0.03	0.01
O=F,Cl	–0.13	–0.45	–0.25	–0.31	–0.16	–0.15
Total	98.76	96.57	98.70	96.07	98.63	99.77
Number of ions on the basis of 24 (O, OH, F,Cl) (apfu)						
Si	5.353	5.657	5.459	5.559	5.462	5.432
Al iv	2.647	2.343	2.541	2.441	2.538	2.568
Al vi	0.841	0.838	0.792	1.326	0.868	0.805
Ti	0.297	0.215	0.277	0.076	0.289	0.308
Cr	0.000	0.004	0.002	0.001	0.010	0.001
Fe^{2+}	3.755	1.380	3.092	2.830	2.394	2.462
Mn	0.090	0.055	0.096	0.103	0.035	0.111
Mg	0.667	3.109	1.378	1.218	1.972	1.952
Zn	0.002	0.007	0.010	0.012	0.006	0.007
Ca	0.002	0.003	0.002	0.001	0.002	0.001
Na	0.026	0.022	0.014	0.009	0.023	0.008
K	1.864	1.828	1.855	1.820	1.885	1.842
Ba	0.000	0.000	0.008	0.000	0.011	0.001
Rb	0.010	0.000	0.010	0.000	0.000	0.000
Cs	0.002	0.000	0.000	0.000	0.000	0.000
OH*	3.848	3.488	3.705	3.625	3.812	3.828
F	0.148	0.510	0.293	0.375	0.179	0.169
Cl	0.004	0.002	0.002	0.000	0.008	0.003
cat sum	15.557	15.461	15.536	15.396	15.495	15.497
Fe/(Fe+Mg)	0.849	0.307	0.692	0.699	0.548	0.558

Sr, Sn, Ga, Ni, Cu were also analyzed but the abundances are below detection limits
* calculated H_2O content

4.2.5. Garnet

Garnet (Tab. 5) is present as an accessory component in several samples, which also contain tourmaline. Garnet in medium-Ca granite SN188 is almandine with 28–32.5 mol. % Sps, *c.* 2.4 mol. % Prp and near 0.5 mol. % Adr.

Granite sample JP13B with muscovite and biotite contains several crystals of garnet per thin section. The core dominated by almandine and spessartine (37.6 mol. % Sps) is overgrown by a 0.1 mm wide rim enriched in Grs (up to 32 mol. %: Fig. 6a). Details of compositional zoning are shown in Figs 6b and c (old core → rim → overgrowth zone – inner part → outer part: $Grs_{1.0 \rightarrow 3.0 \rightarrow 32.0 \rightarrow 7.0}$ $Prp_{3.5 \rightarrow 1.9 \rightarrow 0.5 \rightarrow 1.6}$ $Alm_{55.7 \rightarrow 36.8 \rightarrow 21.3 \rightarrow 31.4}$ $Sps_{37.9 \rightarrow 50.9 \rightarrow 43.7 \rightarrow 54.0}$). Interpretation of this unusual garnet composition is presented in discussion.

4.2.6. Apatite

Apatite occurs in several compositionally distinct generations (Fig. 7; Tab. 6), especially in low-Ca granites: 1) primary fluorapatite; 2) minute anhedral apatite, carrying in part phosphorus released from albite or sodic plagioclase, contains up to 10 mol. % of chlorapatite component in the predominating fluorapatite; 3) very rare hydrothermal hydroxylapatite filling brittle fractures in tourmaline (Fig. 8a, SN164B). Apatite of type (2) has somewhat variable forms of occurrence. Figure 8b shows anhedral apatite aggregates in clusters of newly formed muscovite (sericite).

Albite often encloses tiny apatite grains, scavenging presumably phosphorus released from albite, which could not be analyzed owing to their small size under one micron (Fig. 8b). Such albite grains frequently show microporosity with tiny pores < 3 microns in size, representing < 5 vol. % of albite.

4.2.7. Tourmaline

Tourmaline is present as an accessory or minor phase, typically less than 3 vol. %, in about a quarter of the samples, but sample SN164A contains *c.* 7 vol. % tourmaline. The analyses plot much closer to foitite field

than to schorl end-member composition (Fig. 9a). Iron dominates, but sample JP13A has Fe^{2+}/Mg near unity and one analysis plots already in the dravite field (Fig. 9a). Tourmaline analyses (Tab. 7) indicate a significant X-site vacancy corresponding to 30–40 % of the site (Fig. 9b). As the Ca content in the rocks is low, Na dominates the X-site. Tourmaline is often accompanied by almandine–spessartine garnet.

4.2.8. Andalusite

A single granite sample (SN334A, Suchý vrch) contained accessory andalusite (Fig. 10). The subhedral andalusite crystals exhibit minor Al–Fe^{3+} substitution (Tab. 7). The occurrence is similar to euhedral andalusite crystals in the Mrákotín type muscovite–biotite granite of the Moldanubian Batholith (D'Amico et al. 1981).

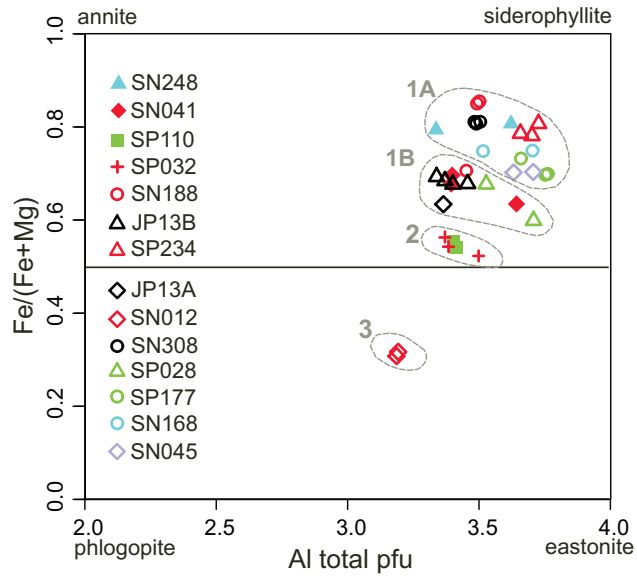

Fig. 5 Biotite analyses in Al total vs. Fe/(Fe + Mg) diagram (apfu).

Tab. 5 Electron-microprobe analyses of garnet (wt. %)

sample	SN188	SN188	SP 156	SP 156	JP13Ba	JP13Ba	JP13Ba	JP13Ba	JP13Ba
analysis	22	30	1	2	19	6	42	5	1
position	core	rim	core	rim	core	rim	overgrowth zone – inner part (aside profile line)	overgrowth zone – inner part	overgrowth zone – outer part
SiO_2	35.80	35.58	36.09	36.84	36.36	36.06	36.99	36.57	36.16
TiO_2	0.01	0.04	0.05	0.02	0.01	0.16	0.31	0.23	0.06
Cr_2O_3	0.00	0.00	0.00	0.01	0.00	0.00	0.00	0.00	0.00
Al_2O_3	20.36	20.37	20.42	20.70	20.36	20.24	20.44	20.31	20.20
FeOt	30.26	28.68	30.38	30.61	25.18	18.86	9.93	13.29	15.88
MnO	12.00	13.63	11.51	11.40	16.59	23.47	19.67	24.18	24.56
MgO	0.59	0.56	0.38	0.39	0.88	0.50	0.12	0.21	0.41
CaO	0.19	0.16	0.21	0.21	0.34	1.10	11.38	5.41	2.52
Na_2O	0.00	0.02	0.00	0.00	0.00	0.00	0.01	0.00	0.00
K_2O	0.00	0.00	0.03	0.01	0.00	0.00	0.02	0.00	0.00
Sc_2O_3	0.02	0.01	0.01	0.00	b.d.l.	b.d.l.	0.00	b.d.l.	b.d.l.
V_2O_3	0.00	0.01	0.02	0.00	b.d.l.	b.d.l.	0.00	b.d.l.	b.d.l.
F	0.00	0.00	b.d.l.	b.d.l.	b.d.l.	b.d.l.	0.16	b.d.l.	b.d.l.
ZrO_2	0.00	0.00	0.00	0.03	b.d.l.	b.d.l.	0.01	b.d.l.	b.d.l.
P_2O_5	0.18	0.31	0.35	0.22	b.d.l.	b.d.l.	0.01	b.d.l.	b.d.l.
Total	99.41	99.36	99.45	100.45	99.71	100.39	99.03	100.20	99.80
Number of atoms (per 12 O) (apfu)									
Si	2.972	2.959	3.002	3.028	2.994	2.956	2.999	2.974	2.970
Ti	0.001	0.002	0.003	0.001	0.000	0.010	0.019	0.014	0.004
Cr	0.000	0.000	0.000	0.000	0.000	0.000	0.000	0.000	0.000
Al	1.993	1.997	2.002	2.006	1.977	1.956	1.953	1.947	1.955
Fe^{3+}	0.062	0.083	0.000	0.000	0.035	0.114	0.014	0.078	0.098
Fe^{2+}	2.039	1.912	2.113	2.104	1.699	1.179	0.659	0.826	0.993
Mn	0.844	0.960	0.811	0.794	1.157	1.629	1.351	1.665	1.708
Mg	0.073	0.069	0.047	0.048	0.108	0.061	0.014	0.025	0.051
Ca	0.017	0.014	0.018	0.018	0.030	0.097	0.988	0.471	0.222
Na	0.000	0.003	0.001	0.000	0.000	0.000	0.001	0.000	0.000
K	0.000	0.000	0.003	0.001	0.000	0.000	0.002	0.000	0.000
End-members (mol %)									
Prp	2.44	2.35	1.57	1.62	3.61	2.04	0.48	0.85	1.70
Alm	68.61	64.68	70.69	70.98	56.75	39.75	21.88	27.64	33.40
Grs	0.57	0.47	0.61	0.62	1.00	3.26	32.81	15.78	7.45
Sps	28.38	32.49	27.13	26.78	38.64	54.95	44.84	55.73	57.45

b.d.l. = below detection limit

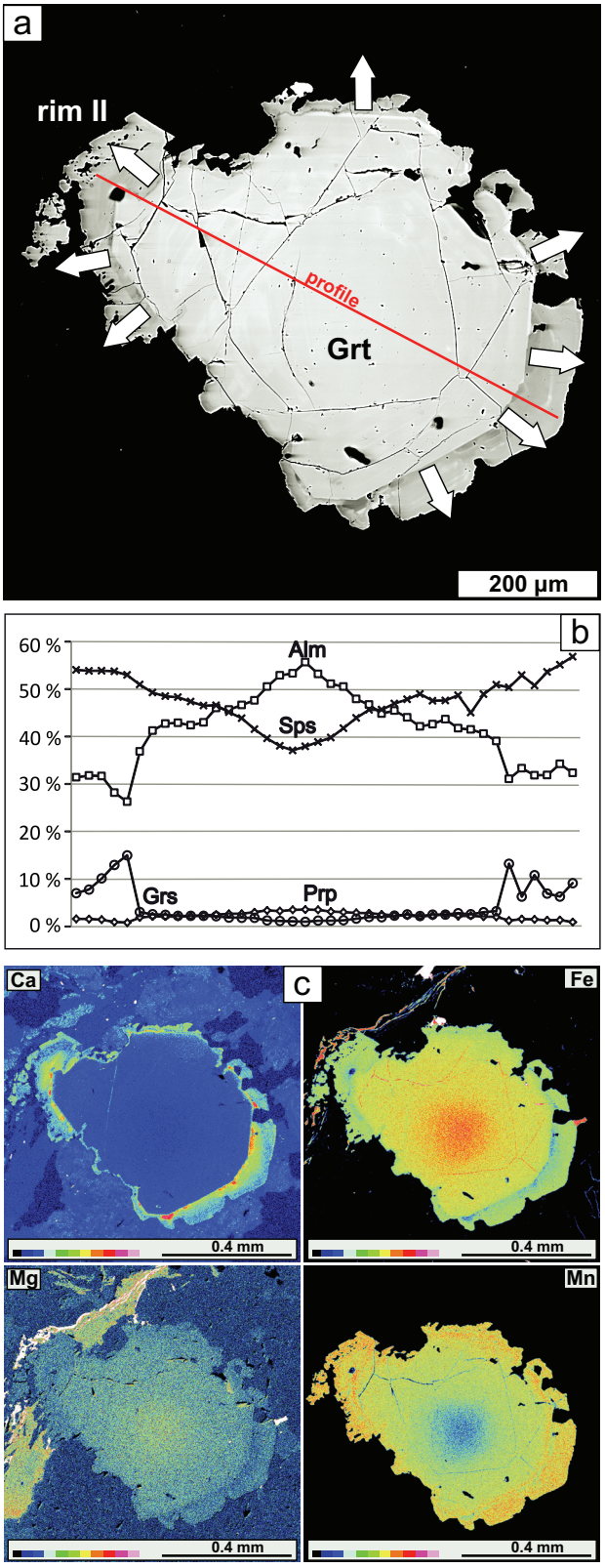

Fig. 6 Zoning of a garnet with grossular-rich rim surrounding a primary Alm–Sps core (sample JP13B, Hrad hill) **a** – Back-scattered electron (BSE) image. Red line illustrates a compositional profile. **b** – Profile of main garnet components (mol. %). **c** – Distribution maps of the main chemical components in garnet.

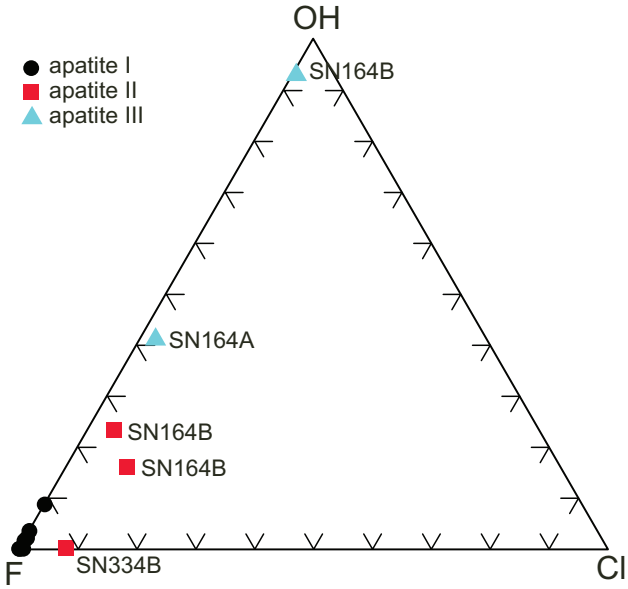

Fig. 7 Chemical composition of apatite in the F–OH–Cl ternary.

Tab. 6 Electron-microprobe analyses of apatite (wt. %)

sample	JP13A	SP165	SN164B	SN164B
analysis	93	83	37	39
SiO_2	0.00	0.00	0.02	0.01
FeOt	0.08	0.06	0.48	0.65
MnO	0.98	0.25	0.85	2.32
MgO	0.02	0.00	0.01	0.00
CaO	54.56	55.22	54.74	52.24
SrO	0.02	0.01	0.00	0.25
Na_2O	0.08	0.01	0.00	0.09
P_2O_5	42.20	41.59	41.12	40.85
F	3.75	3.40	2.73	0.24
Cl	0.02	0.01	0.71	0.05
La_2O_3	0.07	0.00	0.00	0.00
Ce_2O_3	0.04	0.00	0.05	0.00
Nd_2O_3	0.07	0.00	0.00	0.00
Y_2O_3	0.00	0.01	0.05	0.00
H_2O*	0.00	0.16	0.29	1.62
Total	101.88	100.70	101.05	98.31
Number of ions on the basis of 13 (O, OH, F, Cl) (apfu)				
Si	0.000	0.000	0.002	0.001
Fe^{2+}	0.005	0.004	0.034	0.047
Mn	0.070	0.018	0.061	0.169
Mg	0.002	0.000	0.002	0.000
Ca	4.908	5.015	4.990	4.819
Sr	0.001	0.000	0.000	0.013
Na	0.013	0.001	0.000	0.015
P	3.000	2.984	2.962	2.977
F	0.997	0.911	0.735	0.064
Cl	0.002	0.001	0.103	0.007
La	0.002	0.000	0.000	0.000
Ce	0.001	0.000	0.002	0.000
Nd	0.002	0.000	0.000	0.000
Y	0.000	0.001	0.002	0.000
OH	0.001	0.088	0.162	0.929

Pb, Pr, S were also analyzed but the abundances are below detection limits

* H_2O calculated from stoichiometry

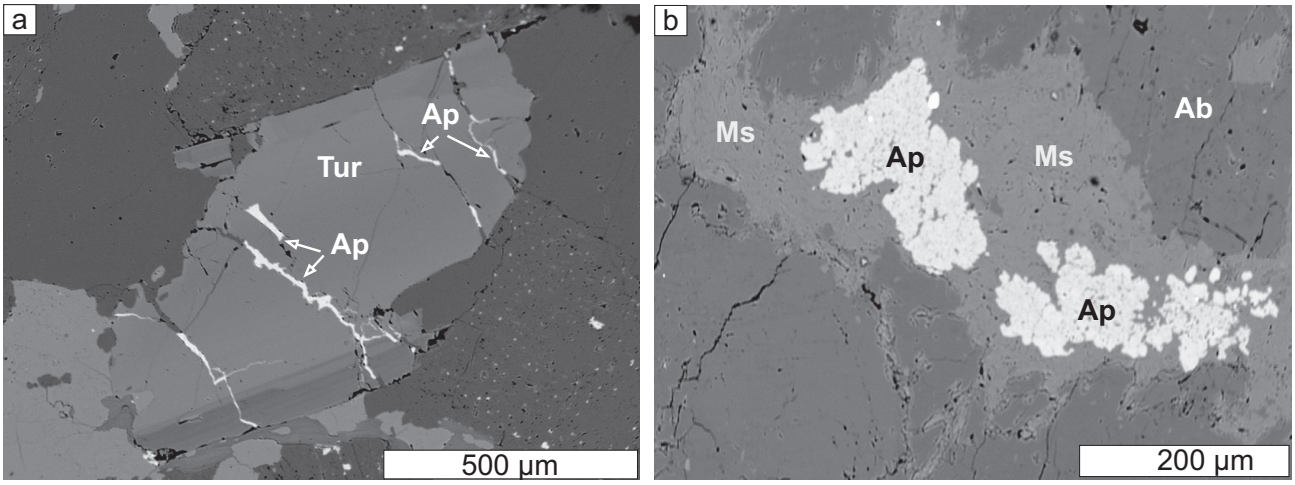

Fig. 8 Back-scattered electron images of apatite. **a** – Hydroxylapatite (Ap, apatite III) filling fractures in schorl (Tur). The tiny white particles in the bottom right corner are apatite II, unmixed from albite. Sample SN164B, Nad Skalným. **b** – Fine-grained remobilized apatite (Ap, probably of a 2nd generation) in aggregates of newly formed muscovite (Ms) in albite (Ab). Sample SN308, Hodňov.

4.2.9. Beryl

Several samples contain newly formed beryl in pinite pseudomorphs (muscovite + chlorite) after cordierite (Fig. 11a). Studies of the beryllium content in cordierites (Povondra and Čech 1978, 1.44 wt. % BeO in Haddam cordierite, USA) and newly formed beryl in pseudomorphs after cordierite (Vrána 1979b; Černý 2002 and references therein) show the tendency of Be to enter cordierite and later to unmix as minute secondary beryl crystals. Our data indicate that Be contents of about 10–20 ppm in whole-rock are sufficient to result in crystallization of minute secondary beryl in pinite pseudomorphs after cordierite (see Tab. 3 for analyses of muscovite and chlorite in pinite). The mineral is documented in samples SN188 (Horní Planá), JP13A (Hrad), SP032 and SP028 (both Studničná Hora). The newly formed beryl contains several minor elements: 0.017–0.030 apfu Fe, 0.036–0.069 apfu Mg and 0.058–0.081 apfu Na (Tab. 7). These contents are much lower compared to low-T beryl studied by Novák et al. (2011).

4.2.10. Bertrandite

Compared to secondary beryl, somewhat different conditions accompanied formation of bertrandite in the sample SP177, Květušín (Fig. 11b). Bertrandite, $Be_4Si_2O_7(OH)_2$,

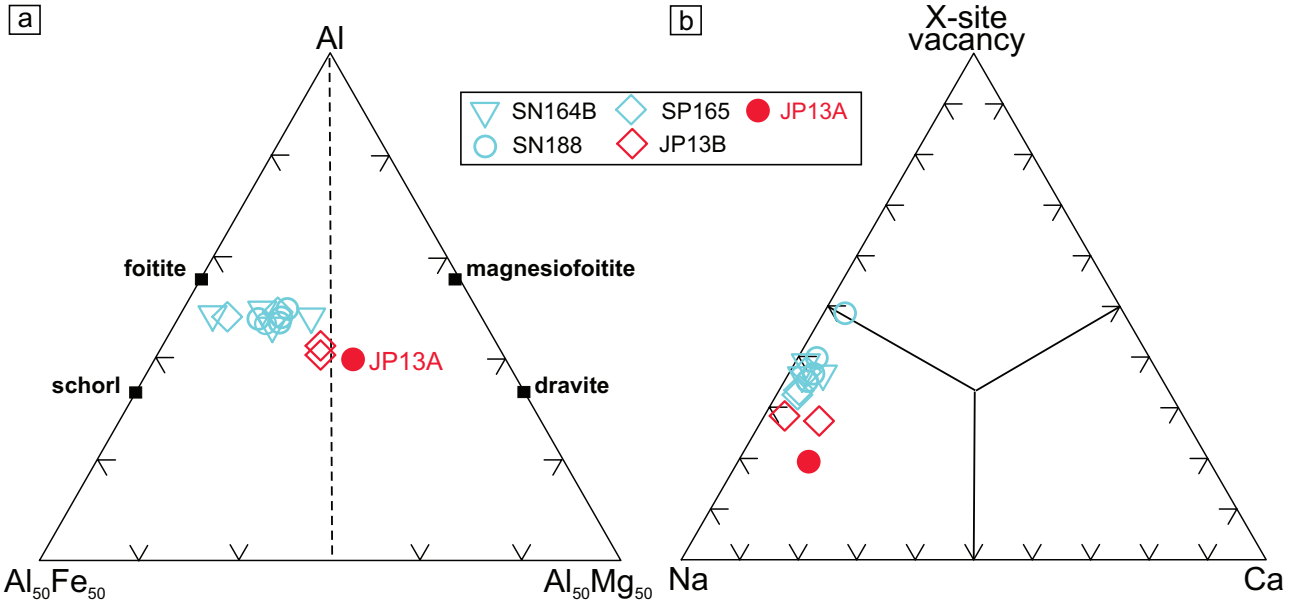

Fig. 9 Compositional variation of tourmaline. **a** – Relations of Al, Fe and Mg atoms; **b** – Ternary plot Na–X-site vacancy–Ca (apfu).

Tab. 7 Electron-microprobe analyses of tourmaline, rutile, beryl and andalusite (wt. %)

mineral	Tur	Tur	Tur	Rt	Rt	Rt	Brl	Brl	And	And
sample	SN164B	SP165	SN188	SN334B	SN334B	SN334A	SN188	SP032	SN334A	SN334A
analysis	32	76	19	6	8	48	26	42	45	46
SiO_2	34.19	34.46	35.75	b.d.l.	b.d.l.	b.d.l.	66.30	68.10	36.61	36.71
TiO_2	0.13	0.73	0.59	89.66	95.65	92.29	b.d.l.	b.d.l.	0.11	0.03
Al_2O_3	34.57	34.16	34.96	0.11	0.07	0.16	17.75	18.20	61.79	61.74
Cr_2O_3	0.00	0.02	0.02	b.d.l.	b.d.l.	b.d.l.	b.d.l.	b.d.l.	b.d.l.	b.d.l.
FeOt	13.48	12.97	9.94	2.70	1.46	2.40	0.40	0.36	0.48	0.29
MnO	0.17	0.29	0.07	b.d.l.	b.d.l.	b.d.l.	b.d.l.	b.d.l.	b.d.l.	b.d.l.
MgO	0.90	1.37	3.04	b.d.l.	b.d.l.	b.d.l.	0.34	0.52	0.05	0.03
CaO	0.05	0.11	0.17	b.d.l.	b.d.l.	b.d.l.	b.d.l.	b.d.l.	b.d.l.	b.d.l.
Na_2O	1.81	1.86	1.51	b.d.l.	b.d.l.	b.d.l.	0.46	0.40	b.d.l.	b.d.l.
K_2O	0.04	0.01	0.01	b.d.l.	b.d.l.	b.d.l.	b.d.l.	b.d.l.	b.d.l.	b.d.l.
P_2O_5	b.d.l.	b.d.l.	b.d.l.	b.d.l.	b.d.l.	b.d.l.	b.d.l.	b.d.l.	0.04	0.04
ZnO	0.08	0.12	0.00	b.d.l.	b.d.l.	b.d.l.	b.d.l.	b.d.l.	b.d.l.	b.d.l.
Ta_2O_5	b.d.l.	b.d.l.	b.d.l.	1.65	0.20	0.98	n.a.	n.a.	n.a.	n.a.
Nb_2O_5	b.d.l.	b.d.l.	b.d.l.	5.62	2.18	4.44	n.a.	n.a.	n.a.	n.a.
SnO	b.d.l.	b.d.l.	b.d.l.	0.07	b.d.l.	0.06	n.a.	n.a.	n.a.	n.a.
V_2O_3	0.02	0.02	0.01	0.16	0.18	b.d.l.	n.a.	n.a.	n.a.	n.a.
Sc_2O_3	b.d.l.	b.d.l.	b.d.l.	0.30	0.38	0.24	n.a.	n.a.	n.a.	n.a.
ZrO_2	b.d.l.	b.d.l.	b.d.l.	b.d.l.	0.12	b.d.l.	n.a.	n.a.	n.a.	n.a.
BeO	n.a.	n.a.	n.a.	n.a.	n.a.	n.a.	13.76	14.11	n.a.	n.a.
B_2O_3*	10.24	10.33	10.55	n.a.	n.a.	n.a.	n.a.	n.a.	n.a.	n.a.
F	0.41	0.33	0.19	n.a.	n.a.	n.a.	n.a.	n.a.	0.06	0.04
Cl	0.00	0.01	0.00	n.a.	n.a.	n.a.	n.a.	n.a.	n.a.	n.a.
H_2O*	3.34	3.40	3.55	n.a.	n.a.	n.a.	n.a.	n.a.	n.a.	n.a.
O=F	–0.17	–0.14	–0.08	n.a.	n.a.	n.a.	n.a.	n.a.	n.a.	n.a.
Total	99.26	100.06	100.29	100.27	100.24	100.57	99.01	101.69	99.14	98.88
Atoms per given number of oxygen atoms (apfu)										
	31 (O.OH.F)	31 (O.OH.F)	31 (O.OH.F)	2 O	2 O	2 O	18 O	18 O	5 O	5 O
Si	5.802	5.798	5.887	–	–	–	6.018	6.027	0.999	1.003
Ti	0.017	0.092	0.073	0.927	0.968	0.945	–	–	0.002	0.001
Al	6.914	6.774	6.785	0.002	0.001	0.003	1.899	1.902	1.987	1.989
Cr	0.000	0.003	0.003	–	–	–	–	–	–	–
Fe^{3+}	0.000	0.000	0.000	–	–	–	–	–	–	–
Fe^{2+}	1.913	1.825	1.369	0.031	0.016	0.023	0.030	0.021	0.011	0.007
Mn	0.024	0.041	0.010	–	–	–	–	–	–	–
Mg	0.228	0.344	0.746	–	–	–	0.046	0.041	0.002	0.001
Ca	0.009	0.020	0.030	–	–	–	–	–	–	–
Na	0.596	0.607	0.482	–	–	–	0.081	0.065	–	–
K	0.009	0.002	0.002	–	–	–	–	–	–	–
P	–	–	–	–	–	–	–	–	0.001	0.001
Be**	–	–	–	–	–	–	3.000	3.000	–	–
Zn	0.010	0.015	0.000	–	–	–	–	–	–	–
Ta	–	–	–	0.006	0.001	0.004	–	–	–	–
Nb	–	–	–	0.035	0.013	0.027	–	–	–	–
Sn	–	–	–	0.001		0.001	–	–	–	–
V	0.003	0.003	0.001	0.002	0.002		–	–	–	–
Sc	–	–	–	0.004	0.004	0.003	–	–	–	–
Zr	–	–	–	–	0.001		–	–	–	–
B	3.001	3.010	3.000	–	–	–	–	–	–	–
F	0.220	0.176	0.099	–	–	–	–	–	–	–
Cl	0.000	0.003	0.000	–	–	–	–	–	–	–
OH	3.780	3.822	3.901	–	–	–	–	–	–	–

* values calculated from stoichiometry; ** Be calculated to 3 apfu
the BeO content indicated by the ideal beryl formula was used in calculation of the number of atoms
b.d.l. = below detection limit
n.a. = not analyzed

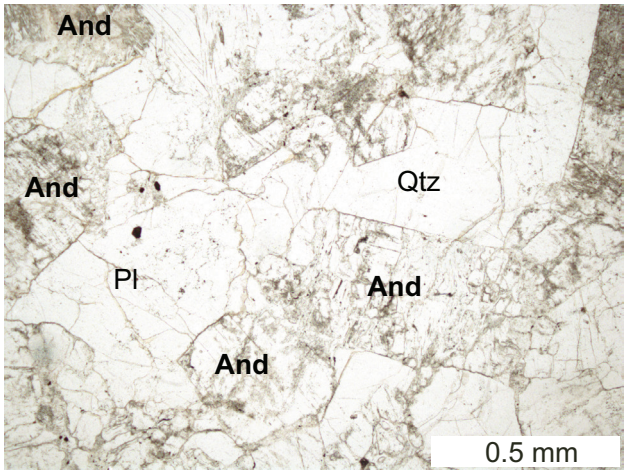

Fig. 10 Local accumulation of subhedral andalusite crystals (And) in muscovite granite. Plane polarized light, sample SN334A, Suchý vrch.

4.3. Whole-rock geochemistry

In general, the studied granites show limited major-element variation (Tabs 8–9). Harker plots (Fig. 13) for medium-Ca granite samples show grouping of TiO_2, Al_2O_3, MgO, P_2O_5 and partly FeOt data points at relatively low SiO_2 values of 71.5–73.5 wt. %. The above listed oxides show lower abundances in low-Ca granites with 73.5–75.7 wt. % SiO_2 (Tab. 8). Surprisingly, A/CNK values correlate positively with SiO_2 in low-Ca granites but they show a broad decrease in medium-Ca granites.

Trace-element multielement patterns of low-Ca granites (Tab. 10), normalized by average values for the upper continental crust (UCC, Taylor and McLennan 1995 Fig. 14a), are characterized by marked depletion (0.1–0.5× UCC), with peaks at 1.0–9.0× UCC for Cs, Rb, K, U and P. Low-Ca granites have low abundances of Ca, Sr, Th, Zr, Y, REE compared to medium-Ca granites

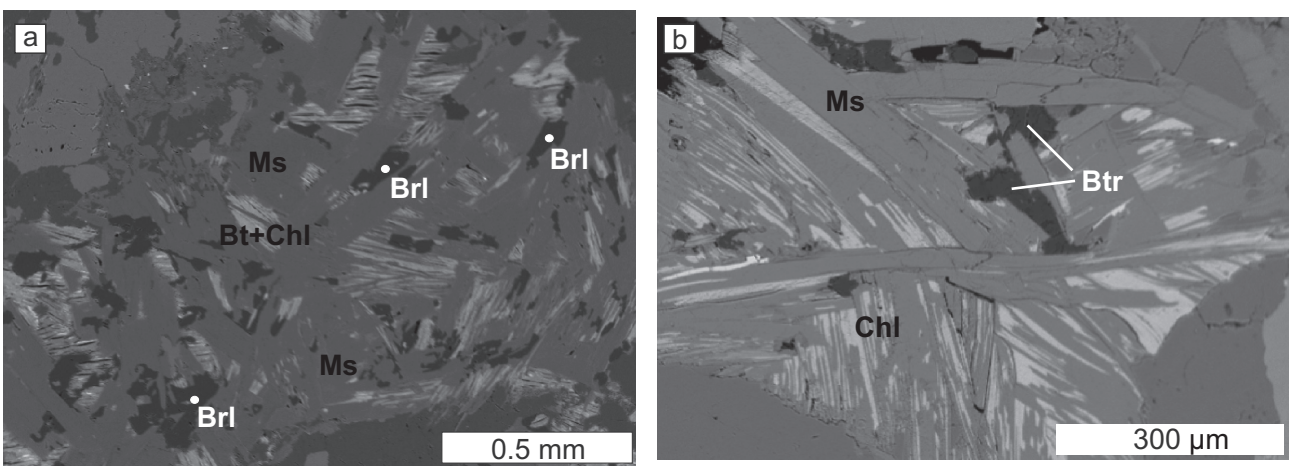

Fig. 11 Beryllium phases in pinite pseudomorph after cordierite **a** – Tiny anhedral beryl (Brl); dark grey is chlorite (Chl), light grey is muscovite (Ms) and biotite (Bt). BSE, sample 188, Horní Planá. **b** – Minute bertrandite (Btr) crystals in pinite pseudomorph. BSE, sample SP177, Květušín.

is seen as dark grains in BSE images of muscovite–chlorite pinite pseudomorphs. In contrast to the secondary beryl, bertrandite is free of Al. Microprobe analyses of bertrandite in sample SP177 gave 48.62 wt. % SiO_2, 0.28 CaO, 0.06 FeOt, 0.11 Na_2O, total 49.07 wt. %.

4.2.11. Niobian rutile

Niobian rutile (Fig. 12) with a strong patchy compositional zoning (sample SN334B, Suchý vrch) is a relatively rare accessory mineral. The majority of the granites in the set of 25 samples contain 1–10 ppm Nb. The sample SN334B contains 6.5 ppm Nb and 1.8 ppm Ta. The highest Nb content in rutile is 0.035 apfu (4.94 wt. % Nb_2O_3) and Ta 0.006 apfu (1.65 wt. % Ta_2O_5).

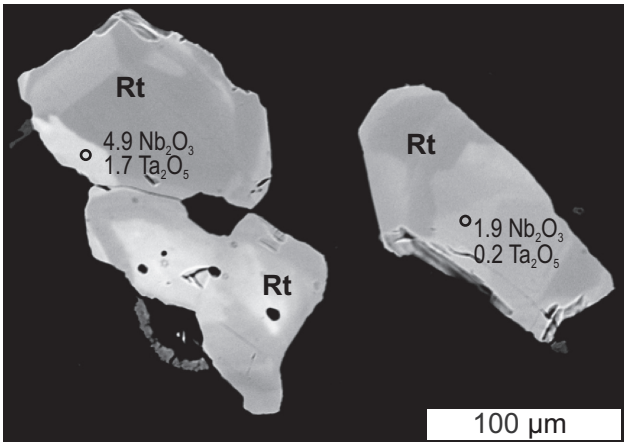

Fig. 12 Accessory niobian rutile with a strong patchy zoning. BSE, sample SN334B, Suchý vrch.

Tab. 8 Major-element analyses of low-Ca granites (wt. %)

sample	SP069	SP011C	SP156	SN045	SP234	SN040	SP248	SN127	SN164A	SN164B	SN188	SN165	SN308	SN334A	SN334B
laboratory	B	A	B	B	B	B	B	B	B	B	B	B	B	B	B
SiO_2	74.77	74.28	75.66	74.60	75.05	73.94	74.78	74.00	71.71	72.62	73.52	74.49	73.62	74.46	74.24
TiO_2	0.08	0.05	0.01	0.05	0.05	0.06	0.05	0.06	< 0.01	< 0.01	0.03	0.06	0.08	0.04	0.06
Al_2O_3	14.56	14.22	14.24	14.01	13.99	14.47	13.96	14.21	15.80	15.32	14.48	14.33	14.45	14.40	14.31
Fe_2O_3	0.33	–	0.55	0.39	0.77	0.44	0.19	0.24	0.37	0.28	0.28	0.46	0.34	0.16	0.08
FeO	0.48	1.16**	0.16	0.50	< 0.03	0.64	0.48	0.56	0.36	0.28	0.64	0.40	0.53	0.40	0.60
MnO	0.074	0.050	0.061	0.051	0.033	0.051	0.030	0.035	0.017	0.021	0.170	0.046	0.037	0.038	0.041
MgO	0.10	0.10	0.13	0.13	0.17	0.24	0.15	0.20	0.12	0.08	0.09	0.16	0.15	0.15	0.22
CaO	0.48	0.41	0.35	0.56	0.59	0.65	0.41	0.60	0.47	0.52	0.43	0.43	0.61	0.48	0.59
Li_2O	0.011	–	0.006	0.004	0.026	0.006	0.011	0.007	0.001	0.002	0.003	< 0.001	0.006	0.003	0.006
Na_2O	4.28	4.80	4.02	3.65	3.94	3.48	3.63	3.37	3.44	4.34	4.48	3.79	3.93	3.61	3.78
K_2O	3.65	4.03	3.76	4.75	3.72	4.60	4.33	4.81	6.21	5.14	4.21	4.86	4.62	5.11	5.04
P_2O_5	0.247	0.300	0.154	0.211	0.271	0.357	0.330	0.241	0.400	0.442	0.328	0.230	0.343	0.193	0.204
F	0.065	–	0.054	0.047	0.064	0.063	0.061	0.049	0.049	0.041	0.044	0.043	0.041	0.028	0.021
CO_2	–	–	–	< 0.01	0.01	< 0.01	< 0.01	< 0.01	< 0.01	< 0.01	< 0.01	< 0.01	< 0.01	< 0.01	< 0.01
C(other)	–	–	–	0.081	< 0.010	0.042	0.072	0.047	0.017	0.026	0.028	0.052	0.036	0.026	0.023
S(tot.)	–	–	–	< 0.010	< 0.010	< 0.010	< 0.010	0.011	< 0.010	0.013	0.010	< 0.010	< 0.010	< 0.010	< 0.010
H_2O^+	0.70*	0.60*	0.61*	0.54	0.60	0.73	0.80	0.80	0.54	0.46	0.61	0.45	0.88	0.72	0.65
H_2O^-	0.06	–	0.05	0.12	0.10	0.16	0.08	0.06	0.11	0.07	0.07	0.06	0.15	0.10	0.07
F(eqv)	–	–	–	–0.020	–0.027	–0.027	–0.026	–0.021	–0.021	–0.017	–0.019	–0.018	–0.017	–0.012	–0.009
Total	99.88	100.00	99.82	99.68	99.36	99.90	99.33	99.27	99.60	99.64	99.41	99.83	99.81	99.90	99.93

* loss on ignition
** total Fe as FeO

B = Laboratory of the Czech Geological Survey – Barrandov
A = Acme Analytical Laboratories Ltd. in Vancouver (Canada)

but they contain elevated Cs, Nb and Sn. For medium-Ca granite samples (Tab. 11), the patterns are similar to the low-Ca granites, except for somewhat higher values in the interval 0.1–0.7 for a number of trace elements, for example Ba, Th, Nb or LREE (Fig. 14b).

Numerous specific features are seen in SiO_2 vs. trace-elements diagrams (Fig. 15). The Rb content in most samples of both granite types is confined to a range of 125–200 ppm. Strontium displays a contrast of low abundances in low-Ca granites (5–60 ppm) and elevated abundances in medium-Ca granites (100–140 ppm); however, there is a small subgroup of medium-Ca granites with Sr contents around 60 ppm (at SiO_2 74–75.5 wt. %). Zirconium shows positive correlation with SiO_2 in low-Ca granites, which are low in Zr (1–42 ppm), but a crude negative correlation in medium-Ca granites. A similar contrast is imperfectly indicated for Y and La. The *mg* number in medium-Ca granites declines with increasing SiO_2, but for low-Ca granites there is limited variation and no clear relationship.

Niobium content is mostly lower than 10 ppm and that of Sn is less than 15 ppm. Beryllium contents vary from 2 to 20 ppm, with one exception of 38 ppm Be (sample SP028, Studničná Hora).

Classification based on Pb and Ba contents (Finger and Schiller 2012) is useful as it indicates division of the studied samples in three groups (Fig. 16a): 1) low-Ca granites, 2) medium-Ca granites of the Smrčina type and 3) other medium-Ca granites. Following Finger and Schiller (2012), the observed variation is interpreted as pointing to a lower temperature of melting in case of the first group.

Apparent lack of a positive correlation between K_2O and Rb is another specific feature of majority of these granites (Fig. 16b).

The REE analyses of low-Ca and medium-Ca granite types are shown in Tabs 12 and 13; three plots showing the total REE contents, La_N/Yb_N ratios and Eu/Eu* values are included as an electronic supplement. The chondrite-normalized patterns (Boynton 1984) exhibit surprising variability (Fig. 17). The total REE contents, La_N/Yb_N ratios and Eu/Eu* values were used to classify the 25 REE distribution diagrams into five major types (Fig. 17): type 1 – minor positive Eu anomaly and relatively high total REE con-

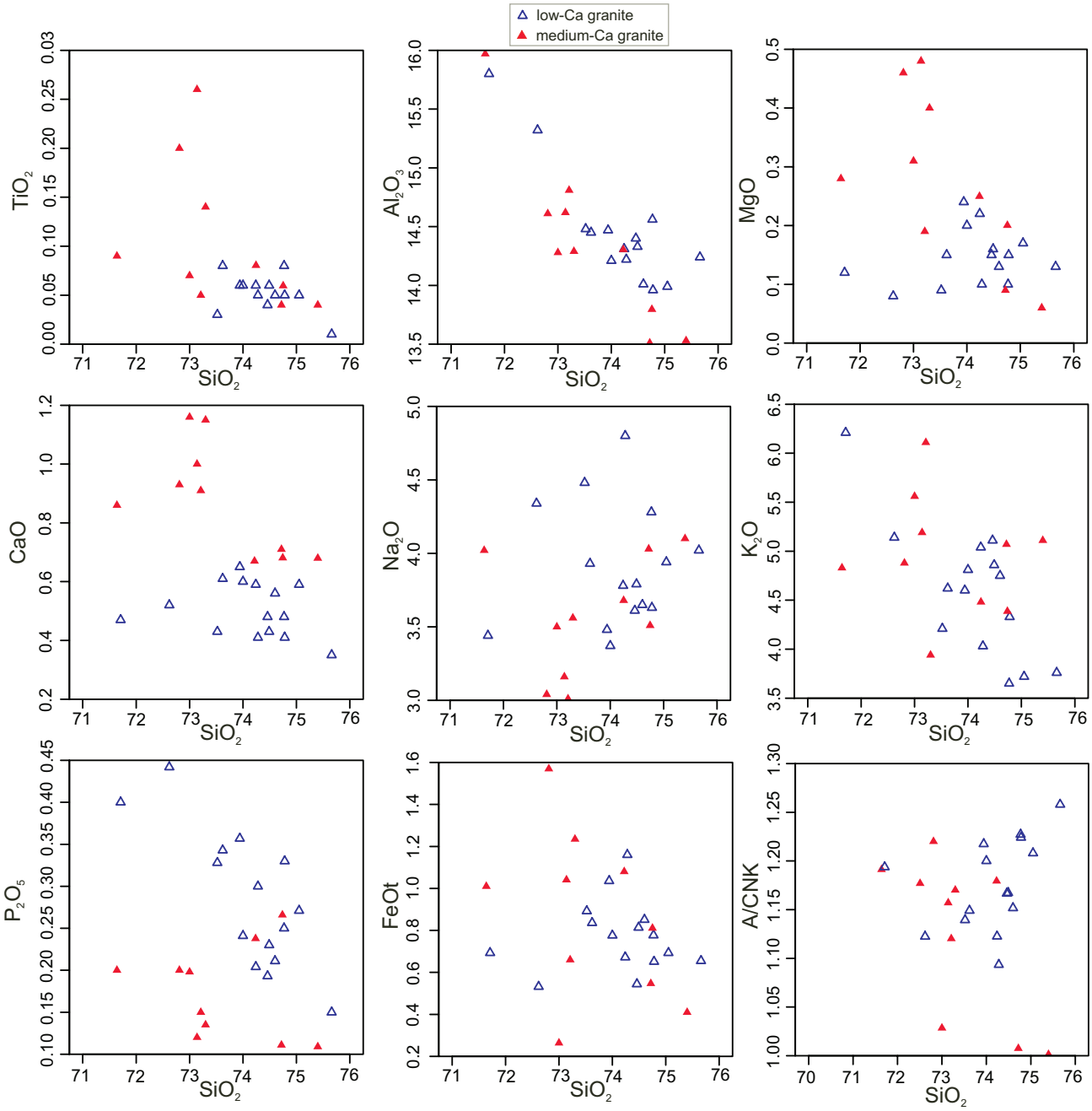

Fig. 13 Harker plots and diagram SiO_2 vs. A/CNK.

tents (n = 3); type 2 – highest REE contents, high La_N/Yb_N ratios (n = 3); type 3 – moderate to low REE abundances, moderate negative Eu anomaly (n = 9); type 4 – low REE abundances, deep negative Eu anomaly (n = 7); type 5 – very low REE abundances (n = 3).

There are three sample pairs each collected in a single granite (pegmatite) dyke (SN334A, B; JP013A, B; SN164A, B). The former two pairs have closely similar REE distributions, while the third displays distinct, mutually nearly complementary, patterns. The samples SN164A, B indicate that the REE distribution was potentially subject to a single magma batch (Fig. 17, type 5).

Many of the REE patterns (Fig. 17) exhibit a distinct tetrad effect, probably indicating a role of water-rich fluids or fluorine in the evolution of these rocks (Irber 1999).

A Zr/Hf vs. Y/Ho diagram (Fig. 18) according to Bau (1996) shows that medium-Ca granites plot in the CHARAC field, whereas low-Ca granites show dominantly lower Zr/Hf values. The CHARAC quadrilateral corresponds to carbonaceous chondrite standard ± 30 %.

Tab. 9 Major-element analyses of medium-Ca granites (wt. %)

sample	SP110	SP032	SP028	SP033	SP177	SN168	SN012	SN041A	JP013A	JP013B
laboratory	B	A	A	A	B	B	B	B	B	B
SiO_2	73.14	73.21	71.64	72.81	74.23	74.75	73.00	73.30	75.40	74.72
TiO_2	0.26	0.05	0.09	0.20	0.08	0.06	0.07	0.14	0.04	0.04
Al_2O_3	14.62	14.81	15.97	14.61	14.30	13.80	14.28	14.29	13.53	13.51
Fe_2O_3	0.59	–	–	–	0.43	0.14	0.06	0.25	< 0.01	0.03
FeO	0.51	0.66**	1.01**	1.57**	0.69	0.68	0.21	1.01	0.41	0.52
MnO	0.027	0.03	0.06	0.06	0.048	0.037	0.019	0.036	0.027	0.043
MgO	0.48	0.19	0.28	0.46	0.25	0.20	0.31	0.40	0.06	0.09
CaO	1.00	0.91	0.86	0.93	0.67	0.68	1.16	1.15	0.68	0.71
Li_2O	0.003	–	–	–	0.031	0.011	0.008	0.008	< 0.001	< 0.001
Na_2O	3.16	3.01	4.02	3.04	3.68	3.51	3.50	3.56	4.10	4.03
K_2O	5.19	6.11	4.83	4.88	4.48	4.38	5.56	3.94	5.11	5.07
P_2O_5	0.119	0.15	0.20	0.20	0.237	0.266	0.198	0.135	0.109	0.111
F	0.052	–	–	–	0.064	0.047	0.039	0.042	0.023	0.021
CO_2	–	–	–	–	< 0.01	< 0.01	< 0.01	< 0.01	< 0.01	< 0.01
C(other)	–	–	–	–	0.023	< 0.010	0.035	0.042	0.034	0.027
S(tot.)	–	–	–	–	< 0.010	< 0.010	< 0.010	< 0.010	< 0.010	< 0.010
H_2O^+	0.57*	0.70*	1.00*	1.10*	0.64	0.67	0.46	0.82	0.30	0.39
H_2O^-	0.10	–	–	–	0.08	0.15	0.15	0.09	0.06	0.08
F(eqv)	–	–	–	–	–0.027	–0.020	–0.016	–0.018	–0.010	–0.009
Total	99.82	99.83	99.96	99.86	99.91	99.37	99.04	99.19	99.88	99.39

* loss on ignition
** total Fe as FeO
B = Laboratory of the Czech Geological Survey – Barrandov
A = Acme Analytical Laboratories Ltd. in Vancouver (Canada)

Two medium-Ca granite samples plotting at lower Zr/Hf value ~ 20 belong to the same dyke.

5. Discussion

5.1. Geochemistry

The studied granite/leucogranite suite includes peraluminous, S-type muscovite–biotite rocks. The single biotite granite sample is of exceptional occurrence. Geochemical investigation leads to division into two major groups of granites: a) low-Ca rich in albite and b) medium-Ca dominated by oligoclase. Phosphorus shows variable partitioning among plagioclase, K-feldspar and apatite.

Separation of our two granite types in the Ba–Rb–Sr diagram (Fig. 2b) and in the Zr/Hf vs. Y/Ho plot (Fig. 18) as well as the contrasting trends in the SiO_2–A/CNK plot (Fig. 13) support the rationale of the division to low-Ca granite and medium-Ca granite.

Low Zr contents most of the studied granites (1–42 ppm) indicate low temperatures of crystallization (Miller et al. 2003) or even Zr undersaturation.

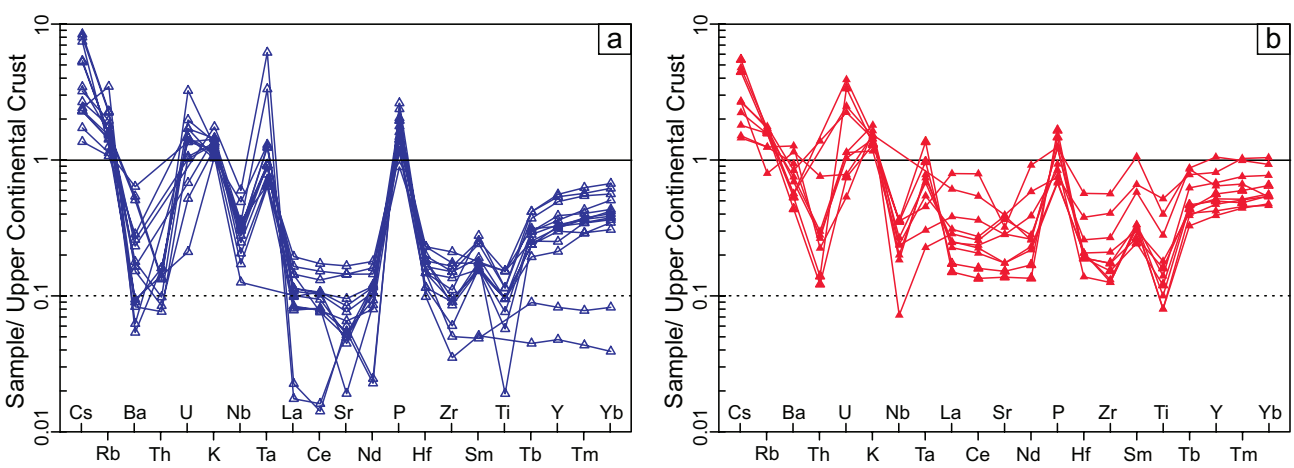

Fig. 14 Trace-element abundances of granite samples normalized by average composition of upper continental crust (Taylor and McLennan 1995) for low-Ca (**a**) and medium-Ca (**b**) granites.

Tab. 10 Trace-element analyses of low-Ca granites (except REE, ppm)

sample	SP069	SP011C	SP156	SN045	SP234	SN040	SP248	SN127	SN164A	SN164B	SN188	SN165	SN308	SN334A	SN334B
laboratory	B	A	B	ACT	ACT	ACT	ACT	ACT	ACT	ACT	ACT	ACT	ACT	ACT	ACT
Cr	n.a.	n.a.	8	< 20	< 20	< 20	< 20	< 20	< 20	< 20	< 20	< 20	< 20	< 20	< 20
Sc	n.a.	1	10	n.a.	n.a.	n.a.	n.a.	n.a.	n.a.	n.a.	n.a.	n.a.	n.a.	n.a.	n.a.
Mo	n.a.	0.1	n.a.	< 2	< 2	< 2	< 2	< 2	< 2	< 2	< 2	< 2	< 2	< 2	< 2
Cu	0	2.8	n.a.	< 10	< 10	< 10	< 10	< 10	< 10	160	10	20	< 10	< 10	10.0
Pb	3	1.5	15	32	37	30	22	33	28	33	18	< 5	31	45	49
Zn	25	18	n.a.	< 30	< 30	< 30	< 30	< 30	60	160	< 30	< 30	30	< 30	< 30
Ni	2	10.1	5	< 20	< 20	< 20	< 20	< 20	< 20	< 20	< 20	< 20	< 20	< 20	< 20
As	3	14.8	n.a.	< 5	< 5	8	< 5	< 5	< 5	< 5	< 5	< 5	7	< 5	< 5
Sb	n.a.	n.a.	0.1	< 0.2	< 0.5	< 0.2	0.3	< 0.2	< 0.2	< 0.2	< 0.2	< 0.2	< 0.2	< 0.2	< 0.2
Bi	3	2.5	2	4.5	2.1	2.8	0.5	1.0	< 0.1	0.6	1.3	< 0.1	2.2	0.4	0.2
Ag	n.a.	n.a.	n.a.	< 0.5	< 0.5	< 0.5	< 0.5	< 0.5	< 0.5	< 0.5	< 0.5	< 0.5	< 0.5	< 0.5	< 0.5
Tl	0.3	0.2	n.a.	0.87	1.1	0.85	1.37	0.89	0.98	0.9	1.26	0.17	0.83	0.71	0.72
Ge	n.a.	n.a.	n.a.	2.6	3	3.3	3.6	3.4	4.7	5.1	5.5	< 0.5	3.9	3.3	3.1
Ba	52	31	55	48	103	260	88	312	134	95	36	17	150	164	368
Be	19	2	5	8	5	5	4	5	3	3	4	3	5	8	11
Co	1	1.4	10	< 1	< 1	< 1	< 1	< 1	1	< 1	< 1	< 1	< 1	< 1	< 1
Cs	33	9.4	29	8.9	20.9	5.8	31.2	13.4	10.4	9	12.5	0.3	8.9	5.3	6.7
Ga	18	21.5	16	18	16	16	15	16	20	21	18	< 1	17	15	15
Hf	1	1.1	1	0.7	1.2	1	0.9	1	0.6	0.9	1.1	< 0.1	0.9	0.7	0.9
Nb	13	9.4	3	7.3	8	7.5	8.5	8	15.7	9.2	4.5	0.6	8.1	5.4	6.5
Rb	268	408.5	148	169	184	179	263	188	211	179	230	9	167	126	133
Sn	25	15	n.a.	7	17	12	17	11	5	8	13	< 1	13	2	3
Sr	16	18.2	19	24	28	48	20	53	22	20	7	< 2	31	35	61
Y	8	4.9	6	6.9	9.0	10.5	7.5	11.4	1.1	1.9	8.3	1.8	7.3	7.7	12.9
Ta	3	1.5	n.a.	2.11	2.9	1.57	2.08	2.13	14.3	7.7	1.47	0.01	2.85	1.54	1.81
Th	2	1.8	n.a.	0.86	1.1	1.06	0.95	1.53	0.12	0.12	0.71	0.69	0.88	1.06	1.71
U	4	4.3	1	3.12	5.0	4.78	1.53	5.8	0.57	0.99	1.65	2.45	3.75	5.81	5.04
V	8	n.a.	2	< 5	< 5	< 5	< 5	< 5	< 5	< 5	< 5	< 5	< 5	< 5	< 5
W	3	2.6	n.a.	0.6	3	0.5	2.5	3.4	0.9	0.5	2.1	< 0.5	0.8	2.2	1.7
Zr	35	19.3	42	18	30	31	27	30	7	10	17	1	18	12	22

B = Laboratory of the Czech Geological Survey – Barrandov
A = Acme Analytical Laboratories Ltd. in Vancouver (Canada)
n.a. = not analyzed
ACT = Activation Laboratories Ltd. In Ancaster (Canada)

Tab. 11 Trace-element analyses of medium-Ca granites (except REE, ppm)

sample	SP110	SP032	SP028	SP033	SP177	SN168	SN012	SN041A	JP013A	JP013B
laboratory	B	A	A	A	ACT	ACT	ACT	ACT	ACT	ACT
Cr	11	n.a.	n.a.	n.a.	< 20	< 20	< 20	< 20	< 20	< 20
Sc	7	1	3	3	n.a.	n.a.	n.a.	n.a.	n.a.	n.a.
Mo	n.a.	< 0.1	< 0.1	< 0.1	< 2	< 2	< 2	< 2	< 2	< 2
Cu	n.a.	1.2	0.7	1.4	< 10	< 10	< 10	< 10	30	< 10
Pb	21	7.0	4.1	5.5	35	35	43	36	49	43
Zn	n.a.	12	24	45	< 30	30	< 30	< 30	< 30	< 30
Ni	8	2.6	2.1	2.6	< 20	< 20	< 20	< 20	< 20	< 20
As	3	< 0.5	< 0.5	3.2	< 5	< 5	< 5	< 5	14	14
Sb	0.1	< 0.1	< 0.1	< 0.1	< 0.2	< 0.5	< 0.5	< 0.2	< 0.2	< 0.2
Bi	n.a.	0.2	2.3	0.6	2	1.3	< 0.4	< 0.1	0.2	< 0.1
Ag	n.a.	< 0.1	< 0.1	< 0.1	< 0.5	< 0.5	< 0.5	< 0.5	< 0.5	< 0.5
Tl	n.a.	< 0.1	0.2	0.3	0.94	1	0.7	0.66	1.18	1.36
Ge	n.a.	n.a.	n.a.	n.a.	3.1	3.0	2.0	2.6	2.8	2.7
Ba	633	414	381	462	293	240	701	518	312	311
Be	5	18	38	11	10	6	6	4	4	5
Co	19	1.5	1.1	2.5	< 1	< 1	< 1	1	< 1	< 1
Cs	10	6.7	17.8	9.9	20.4	16.6	5.6	5.4	8.3	10.1
Ga	13	13.5	14.8	16.1	17	16	10	18	15	16
Hf	2	0.8	1.2	3.3	1.1	1.1	1.1	1.5	1.2	1.2
Nb	n.a.	1.8	6.7	8.9	8.8	9	6	5.9	4.6	5
Rb	90	176.4	192.5	198.2	184	178	140	140	175	192
Sn	n.a.	5	9	5	13	13	2	3	6	10
Sr	138	128.0	99.8	112.1	53	48	136	99	61	61
Y	18	11.4	9.3	14.2	12.4	11	15	23.2	8.6	10.4
Ta	n.a.	0.5	1.5	1.0	2.14	3.0	1.2	0.67	1.72	1.63
Th	8	3.2	3.0	14.8	1.49	1.3	2.4	2.84	5.86	6.08
U	2	3.2	2.9	6.3	9.53	2.10	1.5	3.19	12.0	7.32
V	10	8	11	18	< 5	< 5	5	7	< 5	< 5
W	n.a.	0.6	1.5	1.1	2.3	< 1	2	0.6	< 0.5	0.9
Zr	77	23.8	39.9	107.4	33	29	33	51	24	25

B = Laboratory of the Czech Geological Survey – Barrandov
A = Acme Analytical Laboratories Ltd. in Vancouver (Canada)
ACT = Activation Laboratories Ltd. In Ancaster (Canada)
n.a. = not analyzed

In the Pb vs. Ba diagram (Fig. 16a), the low-Ca granites plot along the field boundary of primary low-T S-type granite (Finger and Schiller 2012). Trend observed for all but two low-Ca granites reflects effects of K-feldspar and biotite fractional crystallization as both elements strongly partition into these minerals.

In terms of Pb–Ba contents, the medium-Ca granite dykes split into two broad groups: 1) muscovite–biotite granite of the Smrčina type, 2) other types of muscovite–biotite and biotite granite. Rocks of the group 1 show high Ba at low-to moderate Pb. Compared with the original diagram (Finger and Schiller 2012), the range of Pb is extended to include three Smrčina-type samples with Pb < 10. The observed variation corresponds to an extensive dehydration melting of Bt–Ms typical of higher-T S-type granite (Finger and Schiller 2012). Also biotites with Mg# 0.32–0.58 correspond to an elevated temperature, especially in comparison with low-Ca granites. Slightly elevated Be contents in the Smrčina-type granite, demonstrated by minute secondary beryl crystals, are consistent with the independent position of this granite type. The rare earth element contents in the Smrčina-type granite are higher and show somewhat variable distribution patterns (Fig. 17, types 1, 2).

Although low Ca-granites are low-T rocks according to several indicators (see above), in Pb–Ba diagram they plot along the dividing line instead of the high-Pb area typical of primary low-T granites (Finger and Schiller 2012). We have no explanation for this situation.

5.2. Comparison with other granites in proximity

Plechý Pluton is the largest granite intrusion next to the area of our study (Fig. 1). Our two major granite types show important differences in abundances of several trace elements compared to granites of the Plechý Plu-

ton (Plechý and Třístoličník types; Pertoldová ed. 2006; Verner et al. 2009; Breiter et al. 2007) (Tab. 14).

Two major groups of two-mica (leuco-) granite occur in the Moldanubian Batholith: Deštná and Eisgarn types (Breiter and Koller 1999; René et al. 2003). Experimental work on biotite stability in peraluminous granitic melts in the source suggests biotite dehydration melting at 830–850 °C for generation of the Eisgarn-type magma. In contrast, the Deštná type production probably involved muscovite breakdown at temperatures significantly lower than 750 °C (René et al. 2008). Some of our low-Ca granites show some REE properties similar to the Deštná granite (type 3 in Fig. 17): Eu/Eu* near 1 and low La_N/Yb_N values (René et al. 2003). Although low-Ca granites show similarities with the Deštná type, they are on average poorer in Ca and more albitic.

The two-mica Eisgarn granite (*c.* 6 km^2 segment) studied by Vrána and Slabý (1996) and Vrána (1998) is positioned along faults in retrogressed biotite–muscovite gneisses of the Kaplice Unit, southwest of Rožmberk nad Vltavou. The granites were affected by a late shearing deformation D_4 and were coeval with extensive albitization, which increased the whole-rock values of Na_2O from 3.5 to 5.0 wt. % (with extremes of 5.8–7 wt. %). Several samples show an increase in elements typical of evolved granite magmas or granite-derived fluids: P, B, Sn, Nb and Be. The high P_2O_5 contents (0.7–1.3 wt. %) gave rise locally to primary Fe–Mg phosphates, sarcopside and graftonite. A second group, enriched in P, Li and Be, relates to a single Li-rich pegmatite dyke. The Li_2O contents of up to 2.3 wt. % are bound in microscopic petalite and spodumene (Vrána and Slabý 1996; Vrána 1998).

Studies of dyke swarm of tourmaline granites around the Vydra Pluton (Žáček and Sulovský 2005) and syenite porphyry dyke swarm in the Kvilda area (Žáček et al. 2009) provide additional examples of the regional variation in geochemistry of granitoid dykes in the Bohemian Forest area farther northwest.

Leucocratic muscovite–tourmaline granite dykes around Vydra Pluton (Žáček and Sulovský 2005) are rather similar in composition with our low-Ca granites (Tab. 14). On the other hand, the Kašperské Hory dyke swarm of melasyenite porphyries (Tab. 14) corresponds to composition of melagranitoids (durbachites) (Žáček et al. 2009) that are, consequently, very different from our set of samples.

We have also compared data on our dykes with results of Koller et al. (1987) on granite dykes in diorites in northern Waldviertel. The stronger represented their type 1 group includes biotite rocks with composition of alkali granite, quartz syenite and quartz monzonite, according De La Roche et al. (1980) classification. The rocks contain somewhat elevated K-feldspar and lower quartz

Tab. 12 REE analyses of low-Ca granites (ppm)

sample	SP069	SP011C	SP156	SN045	SP234	SN040	SP248	SN127	SN164A	SN164B	SN188	SN165	SN308	SN334A	SN334B
laboratory	B	A	B	ACT	ACT	ACT	ACT	ACT	ACT	ACT	ACT	ACT	ACT	ACT	ACT
La	3.1	4.5	3.2	2.65	3.40	4.24	2.55	4.55	0.71	0.55	2.47	0.90	3.57	3.57	6.13
Ce	7.2	5.1	6.3	5.24	6.90	8.75	5.40	8.79	0.95	1.08	5.45	2.15	7.14	7.04	11.60
Pr	0.73	0.66	0.81	0.62	0.82	1.05	0.65	1.12	0.17	0.18	0.68	0.28	0.86	0.81	1.33
Nd	3.2	2.9	3.3	2.18	2.90	3.97	2.54	3.95	0.67	0.62	2.34	1.05	3.16	3.21	4.90
Sm	0.82	0.72	0.84	0.77	0.90	1.11	0.74	1.14	0.24	0.23	0.73	0.36	0.84	0.75	1.31
Eu	0.07	0.06	0.05	0.103	0.160	0.292	0.105	0.328	0.104	0.063	0.055	0.017	0.203	0.188	0.361
Gd	0.78	0.58	0.75	0.68	1.00	1.12	0.73	1.15	0.18	0.27	0.83	0.36	0.87	0.80	1.30
Tb	0.21	0.13	0.17	0.16	0.20	0.24	0.16	0.25	0.03	0.06	0.20	0.06	0.17	0.19	0.28
Dy	1.22	0.74	0.99	1.08	1.60	1.67	1.11	1.77	0.18	0.39	1.39	0.36	1.17	1.28	2.06
Ho	0.21	0.15	0.20	0.23	0.30	0.34	0.24	0.36	0.03	0.06	0.27	0.06	0.25	0.25	0.43
Er	0.73	0.46	0.61	0.63	0.90	0.95	0.69	1.09	0.09	0.17	0.83	0.17	0.75	0.78	1.24
Tm	0.13	0.10	0.12	0.101	0.140	0.157	0.119	0.189	0.015	0.027	0.149	0.026	0.127	0.127	0.217
Yb	0.93	0.80	0.87	0.71	1.00	1.11	0.84	1.30	0.09	0.19	1.17	0.16	0.97	0.89	1.55
Lu	0.13	0.12	0.13	0.102	0.150	0.161	0.124	0.192	0.011	0.026	0.174	0.02	0.15	0.138	0.232

B = Laboratory of the Czech Geological Survey – Barrandov
A = Acme Analytical Laboratories Ltd. in Vancouver (Canada)
ACT = Activation Laboratories Ltd. In Ancaster (Canada)

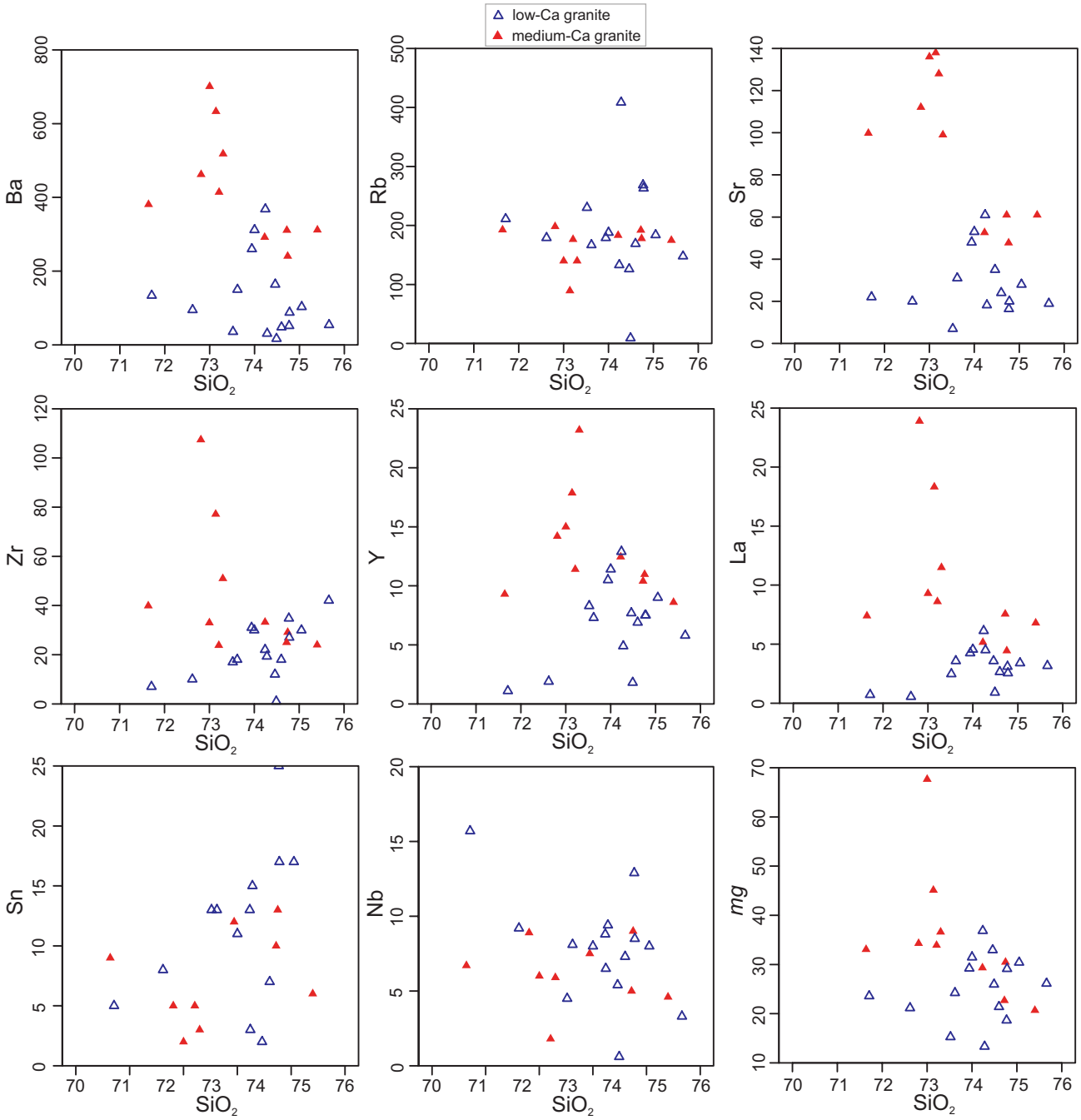

Fig. 15 Binary plots of silica vs. selected trace elements and mg#.

modal contents. The information points to additional variability of dyke rocks in the wider region.

The data obtained indicate that our suite of dyke rocks and minor intrusions is rather unique. At the same time it is noted that a detailed comparison of pluton-size granite masses, such as Deštná granite and Plechý Pluton, with relatively small dykes of this study has some limitations. In the absence of radiogenic isotope data and geochronological dating we prefer not to push the interpretation too far.

5.3. Late-magmatic influx of fluids enriched in Ca and Mg

Tourmaline analysed in most of the samples has a strong prevalence of Fe over Mg. In contrast, sample JP13B (Hrad hill) contains minor tourmaline with Fe/Mg ratio near unity. One analysis even straddles the boundary of the dravite field. Rare accessory garnet in the same sample has a rim enriched in grossular (up to 32 mol. % Grs). As this granite dyke occurs near a contact with

Tab. 13 REE analyses of medium-Ca granites (ppm)

sample	SP110	SP032	SP028	SP033	SP177	SN168	SN012	SN041A	JP013A	JP013B
laboratory	B	A	A	A	ACT	ACT	ACT	ACT	ACT	ACT
La	18.3	8.6	7.4	23.9	5.18	4.50	9.30	11.50	6.80	7.55
Ce	34.7	16.4	15.1	50.8	10.20	8.60	17.50	23.10	13.20	14.40
Pr	3.81	2.05	1.78	6.39	1.22	1.01	1.87	2.80	1.53	1.67
Nd	15.2	7.3	6.8	23.9	4.39	3.50	6.70	10.10	5.67	6.00
Sm	2.98	1.51	1.36	4.77	1.20	1.10	1.50	2.61	1.42	1.45
Eu	0.73	0.61	0.52	0.62	0.363	0.280	0.720	0.688	0.320	0.360
Gd	2.99	1.51	1.35	3.71	1.30	1.20	1.70	2.64	1.13	1.25
Tb	0.50	0.29	0.26	0.55	0.28	0.30	0.40	0.56	0.21	0.25
Dy	3.04	1.78	1.43	2.71	1.91	1.70	2.40	3.70	1.42	1.69
Ho	0.65	0.34	0.30	0.47	0.40	0.40	0.50	0.74	0.29	0.35
Er	2.09	0.98	0.82	1.11	1.17	1.10	1.60	2.12	0.84	1.07
Tm	0.34	0.17	0.15	0.22	0.197	0.160	0.250	0.328	0.146	0.168
Yb	2.30	1.24	1.02	1.18	1.43	1.20	1.70	2.05	1.05	1.19
Lu	0.37	0.18	0.14	0.17	0.214	0.190	0.270	0.268	0.159	0.18

B = Laboratory of the Czech Geological Survey – Barrandov
A = Acme Analytical Laboratories Ltd. in Vancouver (Canada)
ACT = Activation Laboratories Ltd. In Ancaster (Canada)

Tab. 14 Comparison of abundances of U, Th, Zr, Rb, Sr and Nb (ppm) in the studied granites and the Plechý Pluton

element	n	U	Th	Zr	Rb	Sr	Nb
Třístoličník granite*	3	7–12	39–47	140–165	364–424	25–144	13–17
Plechý granite*	4	6–9	10–47	49–89	311–350	34–59	14–21
Marginal granite*	2	2–3	7	20–23	211–230	15–44	8–11
Leucocratic Ms granite, dykes near Vydra Pluton+	3	2–9	<2.1	12–37	200–234	23–102	9–14
Albite granites, Rožmberk nad Vltavou**	14	–	–	–	138–595	<42–161	20–148
Medium-Ca granites, this study	10	2–6	2–15	24–107	80–200	61–137	2–9
Low-Ca granites, this study	15	2–10	1–2	1–42	5–268	2–61	3–16
Melasyenite porphyry, Kašperské Hory area++	3	18–20	38	296–356	352–358	294–337	25–29

References: * Pertoldová et al. (2006), + Žáček and Sulovský (2005), ** unpublished report S. Vrána, ++ Žáček et al. (2009)

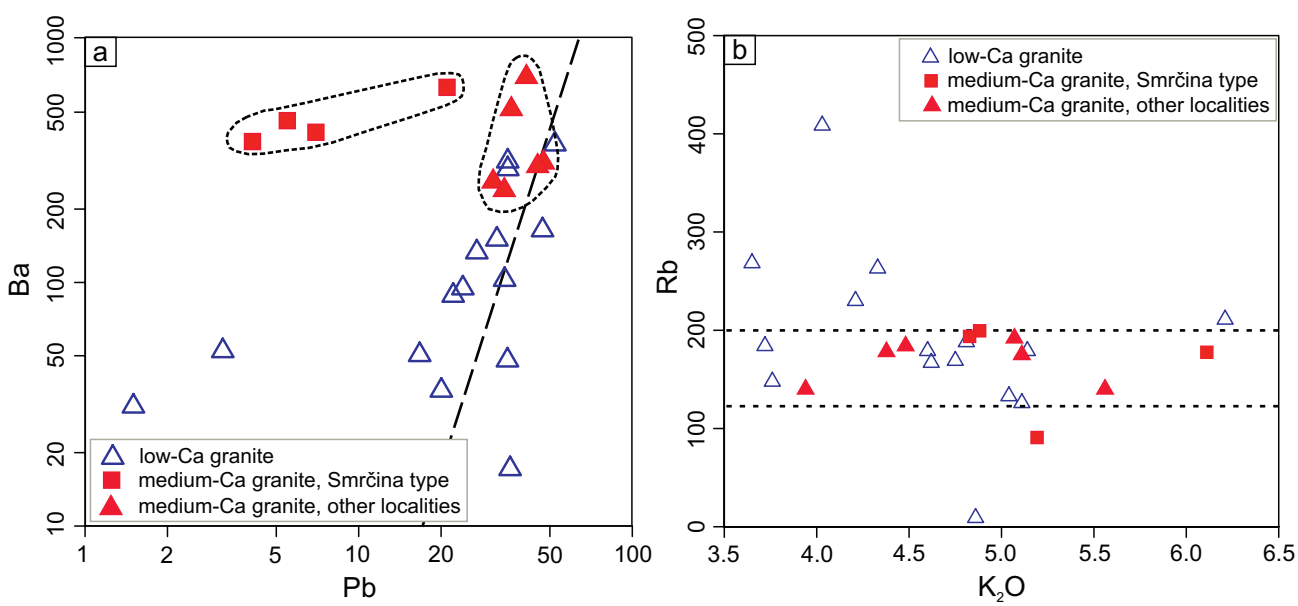

Fig. 16a – Whole-rock Pb vs. Ba diagram (ppm). Dashed line divides relatively low-Pb field of higher temperature granites from high-Pb field of their low-T counterparts (Finger and Schiller 2012). **b** – Variation K_2O (wt. %) vs. Rb (ppm) in the two granite types. Dashed lines indicate limits of 125 and 200 ppm Rb.

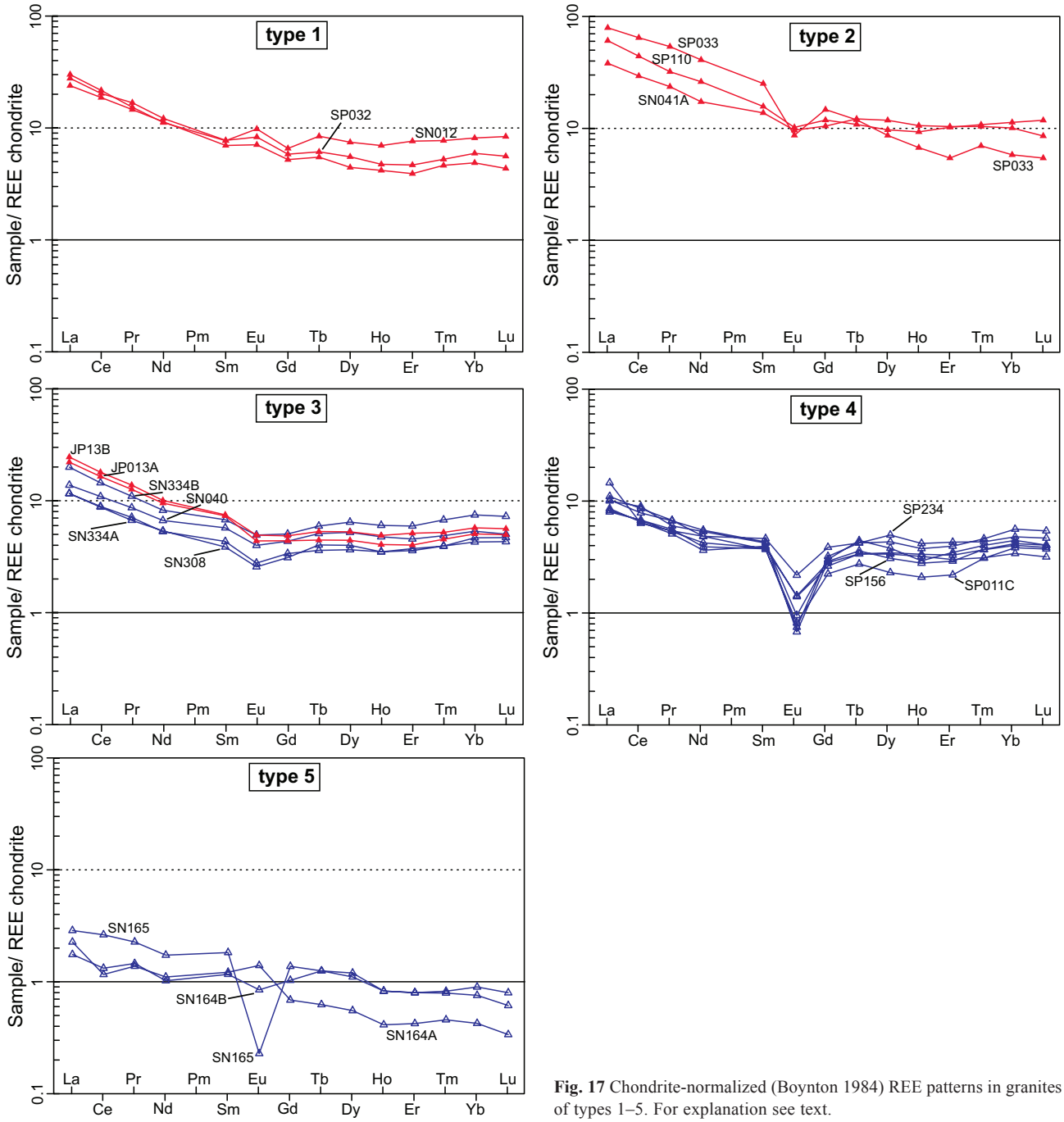

Fig. 17 Chondrite-normalized (Boynton 1984) REE patterns in granites of types 1–5. For explanation see text.

durbachite (hornblende–biotite melagranitoid), the situation may indicate an influx of Mg- and Ca-enriched fluids from the country-rock durbachite into the cooling granite dyke. There is no indication of a late high-pressure event, as an alternative for a high Grs explanation.

5.4. Late- and post-magmatic reactions

Petrographic and mineralogical observations indicate effects of low-T solidus reactions, often involving hydration, which modified the mineralogical composition of granites. They included partial replacement of biotite by muscovite and of plagioclase by muscovite as well as cordierite replacement by chlorite and muscovite to form "pinite" pseudomorphs. The pinitization was sometimes accompanied by crystallization of minor secondary beryl or, alternatively, very rare bertrandite. Partial separation of phosphorus from plagioclase resulted in unmixing of tiny grains of apatite II. This process was significant in that it affected substantial volumes in alkali-feldspar granites, represented by *c.* 30 vol. % of albite. Very common was also low-T chloritization of biotite.

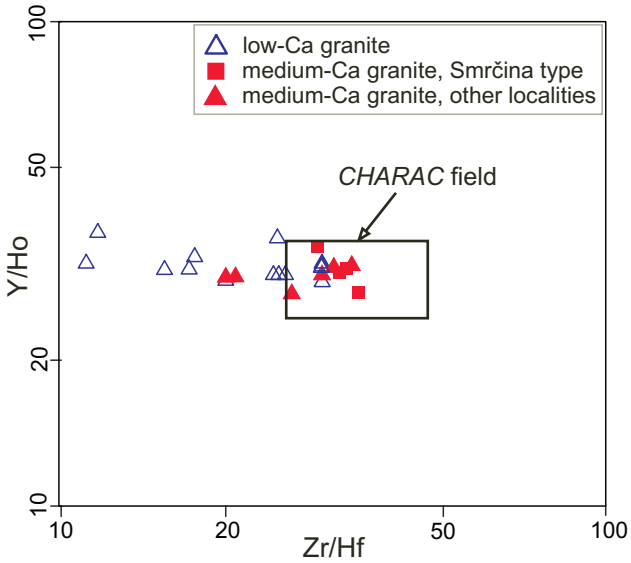

Fig. 18 Plot of Zr/Hf vs. Y/Ho for studied granites. CHARAC field denotes CHAarge-and-RAdius-Controled behaviour of trace elements (Bau 1996).

6. Conclusions

The Moldanubian Zone in S and SW Bohemia (the Horní Planá, Nová Pec and Smrčina areas of the Bohemian Forest) contains numerous granite/leucogranite dykes and small intrusions. The samples of studied biotite–muscovite and biotite granites can be split into two major groups, low-Ca and medium-Ca. The rock suite includes samples containing besides ordinary accessory minerals such as zircon, monazite, ilmenite, apatite and xenotime also Nb-rutile, tourmaline ± garnet, andalusite, secondary beryl or bertrandite in pinite pseudomorphs after cordierite. Rare-earth element analyses indicate five types of the REE distribution with different magnitudes of negative or positive Eu anomalies, variable total REE contents and La_N/Yb_N ratios.

Among medium-Ca granites, relatively independent group represent fine-grained two-mica granites ("Smrčina type"). The Pb vs. Ba diagram indicates relatively high temperatures for the parental melts, as does relatively high-T character of biotite. A specific feature of the Smrčina granite is a slightly elevated Be content of 5–20 (38) ppm. Beryllium, primarily contained in cordierite, occurs in minute crystals of secondary beryl in pinite pseudomorphs after cordierite.

Low-Ca feldspar granites have low abundances of Ca, Sr, Th, Zr, Y, REE compared to medium-Ca granites but they contain elevated Cs, Nb and Sn. The Zr/Hf ratios are lower than in medium-Ca granites. It is surprising that Rb does not correlate with SiO_2 and K_2O and remains nearly constant within the range of 125–200 ppm. Whole-rock composition of the low-Ca granites indicates a possible origin by K-feldspar ± biotite fractional crystallization. It is likely that the parental magma originated by regional migmatization during the early Bavarian phase, probably near 325 Ma.

Acknowledgements. The study was supported by the internal projects of the Czech Geological Survey Nos 321350 and 321183. Madeleine Štulíková is thanked for revising the English of this manuscript. Our thanks are due to handling editor M. Štemprok and to F. Finger and anonymous as referees. Comments and corrections by the editor V. Janoušek significantly improved the manuscript.

Electronic supplementary material. Three plots showing total whole-rock REE contents, La_N/Yb_N ratios and Eu/Eu* values, are available online at the Journal web site (*http://dx.doi.org/10.3190/jgeosci.213*).

References

Aftalion M, Bowes DR, Vrána S (1989) Early Carboniferous U–Pb zircon age for garnetiferous, perpotassic granulites, Blanský les Massif, Czechoslovakia. Neu Jb Mineral, Mh 1989: 145–152

Bau M (1996) Controls on the fractionation of isovalent trace elements in magmatic and aqueous systems: evidence from Y/Ho, Zr/Hf, and lanthanide tetrad effect. Contrib Mineral Petrol 123: 323–333

Boynton WV (1984) Cosmochemistry of the rare earth elements; meteorite studies. In: Henderson P (ed) Rare Earth Element Geochemistry. Elsevier, Amsterdam pp 63–114

Breiter K (2010) Geochemical classification of Variscan granitoids in the Moldanubicum (Czech Republic, Austria). Abh Geol B-A 65: 19–25

Breiter K, Koller F (1999) Two-mica granites in the central part of the South Bohemian Pluton. Abh Geol B-A 56: 201–212

Breiter K, Scharbert S (1995) The Homolka Magmatic Centre – an example of Late Variscan ore bearing magmatism in the Southbohemian Batholith (Southern Bohemia, Northern Austria). Jb Geol B-A 138: 9–25

Breiter K, Förster H-J, Škoda R (2005) Extreme P-, Bi-, Nb-, Sc-, U- and F-rich zircon from fractionated phosphorus granites: the peraluminous Podlesí granite system, Czech Republic. Lithos 88: 15–34

Breiter K, Koller F, Scharbert S, Siebel W, Škoda R, Frank W (2007) Two-mica granites of the Plechý (Plöckenstein) Pluton in the triple-point area (Trojmezí, Dreiländereck) of Austria, the Czech Republic and Germany. Jb Geol B-A 147: 527–544

Černý P (2002) Mineralogy of beryllium in granitic pegmatites. In: Grew E (ed) Beryllium: Mineralogy, Petrology, and Geochemistry. Reviews in Mineralogy and Geochemistry 50: pp 405–444

D'Amico C, Rottura A, Bargossi GM, Nannetti MC (1981) Magmatic genesis of andalusite in peraluminous granites, examples from Eisgarn type granites in Moldanubikum. Rc Soc ital Mineral Petrologia 38: 15–25

De La Roche H, Leterrier J, Grandclaude P, Marchal M (1980) A classification of volcanic and plutonic rocks using R_1R_2 – diagram and major-element analyses – its relationship with current nomenclature. Chem Geol 29: 183–210

Dempírová L, Šikl J, Kašičková R, Zoulková V, Křibek B (2010) The evaluation of precision and relative error of the main components of silicate analyses in Central Laboratory of the Czech Geological Survey. Zpr geol výzk v r 2010: 326–330

Fiala J, Matějovská O, Vaňková V (1987) Moldanubian granulites and related rocks: petrology, geochemistry, and radioactivity. Rozpr Čs Akad Věd, ř mat přír Věd 97: 1–102

Fiala J, Fuchs G, Wendt JI (1995) Stratigraphy of the Moldanubian Zone. In: Dallmeyer RD, Franke W, Weber K (eds) Pre-Permian Geology of Central and Eastern Europe. Springer-Verlag, Berlin, pp 417–428

Finger F, Schiller D (2012) Lead contents of S-type granites and their petrogenetic significance. Contrib Mineral Petrol 164: 747–755

Finger F, Roberts MP, Haunschmid B, Schermaier A, Steyrer HP (1997) Variscan granitoids of central Europe: their typology, potential sources and tectonothermal relations. Mineral Petrol 61: 67–96

Finger F, Gerdes A, Janoušek V, René M, Riegler G (2007) Resolving the Variscan evolution of the Moldanubian sector of the Bohemian Massif: the significance of the Bavarian and the Moravo–Moldanubian tectonometamorphic phases. J Geosci 52: 9–28

Frýda J, Breiter K (1995) Alkali feldspars as a main phosphorus reservoirs in rare-metal granites – three examples from the Bohemian Massif (Czech Republic). Terra Nova 7: 315–320

Fuchs G (1976) Zur Entwicklung der Böhmischen Masse. Jb Geol B-A 119: 45–61

Fuchs G, Matura A (1976) Zur Geologie des Kristallins der südlichen Böhmischen Masse. Jb Geol B-A 119: 1–43

Gerdes A, Wörner G, Henk A (2000) Post-collisional granite generation and HT–LP metamorphism by radiogenic heating: the Variscan South Bohemian Batholith. J Geol Soc, London 157: 577–587

Hasalová P, Schulmann K, Lexa O, Štípská P, Hrouda F, Ulrich S, Haloda J, Týcová P (2008) Origin of migmatites by deformation-enhanced melt infiltration of orthogneiss: a new model based on quantitative microstructural analysis. J Metamorph Geol 26: 29–53

Holub FV (1997) Ultrapotassic plutonic rocks of the durbachite series in the Bohemian Massif: petrology, geochemistry and petrogenetic interpretation. Sbor geol Věd, ložisk Geol Mineral 31: 5–26

Holub FV, Klečka M, Matějka D (1995) Igneous activity. In: Dallmeyer RD, Franke W, Weber K (eds) Pre-Permian Geology of Central and Eastern Europe. Springer Verlag, Berlin, pp 444–452

Irber W (1999) The lanthanide tetrad effect and its correlation with K/Rb, Eu/Eu*, Sr/Eu, Y/Ho, and Zr/Hf of evolving peraluminous granite suites. Geochim Cosmochim Acta 63: 489–508

Janoušek V, Bowes DR, Braithwaite CJR, Rogers G (2000) Microstructural and mineralogical evidence for limited involvement of magma mixing in the petrogenesis of a Hercynian high-K calc-alkaline intrusion: the Kozárovice granodiorite, Central Bohemian Pluton, Czech Republic. Trans Roy Soc Edinb, Earth Sci 91: 15–26

Janoušek V, Finger F, Roberts M, Frýda J, Pin C, Dolejš D (2004a) Deciphering the petrogenesis of deeply buried granites: whole-rock geochemical constraints on the origin of largely undepleted felsic granulites from the Moldanubian Zone of the Bohemian Massif. Trans Roy Soc Edinb, Earth Sci 95: 141–159

Janoušek V, Braithwaite CJR, Bowes DR, Gerdes A (2004b) Magma-mixing in the genesis of Hercynian calc-alkaline granitoids: an integrated petrographic and geochemical study of the Sázava intrusion, Central Bohemian Pluton, Czech Republic. Lithos 78: 67–99

Janoušek V, Farrow CM, Erban V (2006) Interpretation of whole-rock geochemical data in igneous geochemistry: introducing Geochemical Data Toolkit (GCDkit). J Petrol 47: 1255–1259

Klomínský J, Jarchovský T, Rajpoot GS (2008) Atlas of Plutonic Rocks and Orthogneisses in the Bohemian Massif, part Moldanubicum. Czech Geological Survey, Prague, pp 1–163

Koller F, Gratzer R, Niedermayr G (1987) Die Ganggesteine in den Dioriten des nördlichen Waldviertels. Ann Naturhist Mus Wien 88 A: 1–21

Košler J, Konopásek J, Sláma J, Vrána S (2013) U–Pb zircon provenance of Moldanubian metasediments in the Bohemian Massif. J Geol Soc, London 171: 83–95

Kröner A, O'Brien PJ, Nemchin AA, Pidgeon RT (2000) Zircon ages for high pressure granulites from South Bohemia, Czech Republic, and their connection to Carboniferous high temperature processes. Contrib Mineral Petrol 138: 127–142

Le Maitre RW (ed.) (2002) A Classification of Igneous Rocks and Glossary of Terms. Blackwell, Oxford, pp 1–193

Liew TC, Hofmann AW (1988) Precambrian crustal components, plutonic associations, plate environment of the Hercynian Fold Belt of Central Europe: indications from a Nd and Sr isotopic study. Contrib Mineral Petrol 98: 129–138

Liew TC, Finger F, Höck V (1989) The Moldanubian granitoid plutons in Austria: chemical and isotopic studies bearing on their environmental setting. Chem Geol 76: 41–55

Medaris GJR, Beard BL, Johnson CM, Valley JW, Spicuzza MJ, Jelínek E, Mísař Z (1995) Garnet pyroxenite and eclogite in the Bohemian Massif: geochemical evidence for Variscan recycling of subducted lithosphere. Geol Rundsch 84: 489–505

Melleton J, Gloaguen E, Frei D, Novák M, Breiter K (2012) How are the emplacement of rare-element pegmatites, regional metamorphism and magmatism interrelated in the Moldanubian domain of the Variscan Bohemian Massif, Czech Republic? Canad Mineral 50: 1751–1773

Miller CF, Meschter McDowell S, Mapes RW (2003) Hot and cold granites? Implications of zircon saturation temperatures and preservation of inheritance. Geology 31: 529–532

Novák M, Gadas P, Filip J, Vaculovič T, Přikryl J, Fojt B (2011) Blue, complexly zoned, (Na,Mg, Fe,Li)-rich beryl from quartz–calcite veins in low-grade metamorphosed Fe-deposit Skály near Rýmařov, Czech Republic. Mineral Petrol 102: 3–14

O'Brien PJ (2008) Challenges in high-pressure granulite metamorphism in the era of pseudosections: reaction textures, compositional zoning and tectonic interpretation with examples from the Bohemian Massif. J Metamorph Geol 26: 235–251

Pertoldová J (ed) (2006) Explanations to the geological map 1:25 000, sheets 32-141 Nové Údolí and 32-142 Nová Pec. Czech Geological Survey, Prague

Pertoldová J, Nahodilová R (eds) (2013) Explanations to the geological map 1:25 000, sheet 32-231 Horní Planá. Czech Geological Survey, Prague

Pouchou J L, Pichoir F (1985) "PAP" φ(ρz) procedure for improved quantitative microanalysis. In: Armstrong JT (ed) Microbeam Analysis. San Francisco Press, San Francisco, pp 104–106

Povondra P, Čech F (1978) Sodium–beryllium-bearing cordierite from Haddam, Connecticut, U.S.A. Neu Jb Mineral, Mh 1978: 203–209

René M, Matějka D, Nosek T (2003) Geochemical constraints on the origin of a distinct type of two-mica granites (Deštná–Lásenice type) in the Moldanubian Batholith (Czech Republic). Acta Montana, Ser A 130: 59–76

René M, Holtz F, Luo C, Beermann O, Stelling J (2008) Biotite stability in peraluminous granitic melts: compositional dependence and application to the generation of two-mica granites in the South Bohemian Batholith (Bohemian Massif, Czech Republic). Lithos 102: 538–553

Schulmann K, Konopásek J, Janoušek V, Lexa O, Lardeaux JM, Edel JB, Štípská P, Ulrich S (2009) An Andean type Palaeozoic convergence in the Bohemian Massif. C R Geosci 341: 266–286

Sláma J, Košler J, Pedersen R (2007) Behaviour of zircon in high-grade metamorphic rocks: evidence from Hf isotopes, trace elements and textural studies. Contrib Mineral Petrol 154: 335–356

Sláma J, Košler J, Condon DJ, Crowley JL, Gerdes A, Hanchar JM, Horstwood MSA, Morris GA, Nasdala L, Norberg N, Schaltegger U, Schoene B, Tubrett MN, Whitehouse MJ (2008) Plešovice zircon – a new natural reference material for U–Pb and Hf isotopic microanalysis. Chem Geol 249: 1–35

Siebel W, Thiel M, Chen F (2006) Zircon geochronology and compositional record of late- to post-kinematic granitoids associated with the Bavarian Pfahl Zone (Bavarian Forest). Mineral Petrol 86: 45–62

Siebel W, Shang CK, Reitter E, Rohrmüller J, Breiter K (2008) Two distinctive granite suites in the SW Bohemian Massif and their record of emplacement: constraints from geochemistry and zircon $^{207}Pb/^{206}Pb$ chronology. J Petrol 49: 1853–1872

Svojtka M, Košler J, Venera Z (2002) Dating granulite-facies structures and the exhumation of lower crust in the Moldanubian Zone of the Bohemian Massif. Int J Earth Sci 91: 373–385

Štípská P, Powell R, Racek M, Lexa O (2014) Intermediate granulite produced by transformation of eclogite at a felsic granulite contact, in Blanský les, Bohemian Massif. J Metamorph Geol 32: 347–370

Taylor SR, McLennan SM (1995) The geochemical evolution of the continental crust. Rev Geophys 33: 241–265

Thiele O (1976) Ein westvergenter kaledonischer Deckenbau im niederösterreichischen Waldviertel. Jb Geol B-A 119: 75–81

Thiele O (1984) Zum Deckenbau und Achsenplan des Moldanubikums der südlichen Böhmischen Masse (Österreich). Jb Geol B-A 126: 513–523

Trubač J, Janoušek V, Vrána S, Wiegand B (2012) Nature, tectonic setting and likely origin of the Palaeoproterozoic (~2.1 Ga) Světlík orthogneisses (southern Bohemia). Miner Slov 44: 110

Verner K, Žák J, Nahodilová R, Holub FV (2008) Magmatic fabrics and emplacement of the cone-sheet-bearing Knížecí stolec durbachite pluton (Moldanubian Unit, Bohemian Massif): implications for mid-crustal reworking of granulitic lower crust in the Central European Variscides. Int J Earth Sci 97: 19–33

Verner K, Žák J, Pertoldová J, Šrámek J, Sedlák J, Trubač J, Týcová P (2009) Magmatic history and geophysical signature of a post-collisional intrusive centre emplaced near a crustal-scale shear zone: the Plechý granite pluton (Moldanubian Batholith, Bohemian Massif). Int J Earth Sci 98: 517–532

Vrána S (1979a) Polyphase shear folding and thrusting in the Moldanubicum of southern Bohemia. Věst Ústř Úst geol 54: 75–86

Vrána S (1979b) A secondary magnesium-bearing beryl in pseudomorphs after pegmatitic cordierite. Čas Mineral Geol 24: 65–69

Vrána S (1998) Large-scale, late magmatic albitization and mineralization of Eisgarn granite concurrent with regional extension deformation of a marginal segment of the Moldanubian Batholith. Acta Univ Carol, Geol 42: 178–180

Vrána S, Slabý J (1996) Regional albitization of granites of the Moldanubian Pluton southwest of Rožmberk nad Vltavou. Zpr o geol výzk za r 1995: 178–179

Vrána S, Šrámek J (1999) Geological interpretation of detailed gravity survey of the granulite complex in southern Bohemia and its structure. Bull Czech Geol Survey 74: 261–277

Vrána S, Janoušek V, Franěk J (2013) Contrasting mafic to felsic HP–HT granulites of the Blanský les Massif (Moldanubian Zone of southern Bohemia): complexity of mineral assemblages and metamorphic reactions. J Geosci 58: 347–378

Wendt JI, Kröner A, Fiala J, Todt W (1993) Evidence from zircon dating for existence of approximately 2.1 Ga old crystalline basement in southern Bohemia, Czech Republic. Geol Rundsch 82: 42–50

Wendt JI, Kröner A, Fiala J, Todt W (1994) U–Pb zircon and Sm–Nd dating of Moldanubian HP/HT granulites from south Bohemia, Czech Republic. J Geol Soc, London 151: 83–90

Whitney DL, Evans BW (2010) Abbreviations for names of rock-forming minerals. Amer Miner 93: 185–187

Žáček V, Sulovský P (2005) The dyke swarm of fractionated tourmaline-bearing leucogranite and its link to the Vydra Pluton (Moldanubian Batholith), Šumava Mts., Czech Republic. J Czech Geol Soc 50: 107–118

Žáček V, Škoda R, Sulovský P (2009) U–Th-rich zircon, thorite and allanite-(Ce) as main carriers of radioactivity in the highly radioactive ultrapotassic melasyenite porphyry from the Šumava Mts., Moldanubian Zone, Czech Republic. J Geosci 54: 343–354

Žák J, Verner K, Finger F, Faryad SW, Chlupáčová M, Veselovský M (2011) The generation of voluminous S-type granites in the Moldanubian Unit, Bohemian Massif, by rapid isothermal exhumation of the metapelitic middle crust. Lithos 121: 25–40

Žák J, Verner K, Janoušek V, Holub FV, Kachlík V, Finger F, Hajná J, Tomek F, Vondrovic L, Trubač J (2014) A plate-kinematic model for the assembly of the Bohemian Massif constrained by structural relationships around granitoid plutons. In: Schulmann K, Martínez Catalán JR, Lardeaux JM, Janoušek V, Oggiano G (eds) The Variscan Orogeny: Extent, Timescale and the Formation of the European Crust. Geological Society, London, Special Publications 405, pp 169–196